Optimization of Tungsten Carbide/MOF Hybrids as Electrochemical Water Splitting Catalysts for HER

By

Umair Sohail

School of Chemical and Materials Engineering

National University of Sciences and Technology

2023

Optimization of Tungsten Carbide/MOF Hybrids as Electrochemical Water Splitting Catalysts for HER

Name: Umair Sohail

Registration No: 00000330333

This thesis is submitted as a partial fulfilment of the requirements for the degree of

MS in Chemical Engineering

Supervisor Name: Dr. Erum Pervaiz

School of Chemical and Materials Engineering (SCME)

National University of Science and Technology (NUST)

H-12, Islamabad, Pakistan

February, 2023

Dedication

By the grace of Almighty Allah, Who is the Most Beneficent and the Most Merciful

This study is dedicated to my parents, who have always been my source of guidance and support.

To my supervisor who shared her knowledge, gave advice, and encouraged me to fulfill my objectives.

And to all my fellows I worked with whom I've enjoyed wonderful memories.

Acknowledgements

There is none other but Almighty Allah, whose will be required for everything and anything in this world, who blessed us with the ability to think and made us willing to explore the entire universe. Infinite greetings to the Holy Prophet Muhammad (PBUH), the cause of the universe's creation and a fountain of knowledge and blessing for all of humanity.

Dr. Erum Pervaiz, my renowned supervisor, deserves credit for trusting in my talents. Her constant guidance, encouragement, and support were vital in the project's success. Author Erum Pervaiz acknowledges NUST Pakistan for providing its research facilities and HEC project marked (2017/HEC/NRPU-10482) for financial assistance.

I'd like to express my gratitude to my deserving GEC members, Dr. Tayyaba Noor and Dr. Ameen Shahid. I've never given it much thought. Having said that, the unwavering moral support that my family and friends have always provided will always be my light in the dark. My heartfelt gratitude goes out to all the personnel and lab attendants. Thank you!

Umair Sohail

Abstract

The depletion of traditional energy supplies, that is, fossil fuels, has increased interest in hydrogen as a source of clean energy. As a fuel, hydrogen boasts a high energy density, carbon-free byproducts, and the ability to be stored. Water splitting is a carbon-neutral method for the sustainable creation of hydrogen. However, the process requires high-performance, stable, and inexpensive catalysts for kinetic and economic viability. Diverse catalysts have been investigated for the effective production of hydrogen through the water splitting process. At operationally relevant current densities, tungsten carbide is a resilient and electrochemically active material with low Tafel slopes and overpotentials equivalent to the standard catalyst platinum. This thesis is to describe the advances that Tungsten carbide and its hybrids have achieved in water-splitting. Particular focus has been given to popular techniques that can enhance the catalytic capabilities of the hybrids for the whole process, beginning with the synthesis procedures and their influence on the structure and properties. In order to determine the optimal class of materials in accordance with hydrogen production procedures, a significant insight into future considerations for catalytic enhancement is also provided for researchers and industry alike.

Table of Contents

Dedication i

Acknowledgements ii

Abstract iii

List of Figures: vi

List of Tables vii

Chapter 1 1

1.1 Background 1

1.2 Electrochemical water splitting (Fundamental Aspects): 5

1.3 Hydrogen Evolution Reaction (HER): 7

1.4 Oxygen Evolution Reaction (OER): 8

1.5 Key Performance Indicators (KPI): 9

1.6 Problem Statement 10

1.7 Research Objective 11

1.8 Scope of Study 11

1.9 Chapter Summary 11

Chapter 2 13

2.1 Literature Review: 13

2.2 Synthesis of Pure Phase WC: 15

2.3 Hydrothermal method: 15

2.2.2 Solid-State Reaction: 19

2.2.3 Chemical Vapor Deposition (CVD) Reaction Synthesis: 21

2.2.4 Synthesis of WC Hybrids: 23

2.3 Electrochemical Activity 26

Chapter 3 31

3.1 Materials:..... 31
3.2 Synthesis of pure Tungsten Carbide (WC): 31
3.3 Synthesis of Pure Prussian Blue (PBNPs): 31
3.4 Synthesis of Pure UiO-66:..... 32
3.5 Synthesis of WC and Prussian blue Hybrids:..... 32
3.6 Synthesis of WC and UIO-66 Hybrids:..... 32
3.7 Preparation of electrode: 33
Chapter 4..... 34
4.1 Material Characterization:..... 34
4.2 Electrochemical Analysis:..... 34
4.3 Results and Discussions: 35
4.3.1 Phase Determination and Crystal Size: 35
4.3.2 Morphological Study and Energy Dispersive X-ray (EDX): 38
4.4 Electrochemical Study:..... 41
4.4.1 Hydrogen Evolution Reaction: 41
4.4.2 Oxygen Evolution Reaction: 43
4.4.3 Cyclic Voltametery:..... 47
4.4.4 Electrochemical Impedance Spectroscopy and Chronopotentiometry:..... 49
4.5 Proposed Mechanism: 52
Conclusion and Future Prospects:..... 54
References:..... 56

List of Figures:

Figure 1: (a) Steam Methane Reforming (b) Coal gasification (c) Water Electrolysis [22] 2
Figure 2: HER and OER reactions of water splitting [69] 6
Figure 3: Synthesis of WC from WO3 precursors [118] 16
Figure 4: Synthesis of WC Nanosheets From Fructose and AMT[122] 18
Figure 5: Synthesis of WC from AMT and Glucose [123] 18
Figure 6**:** Synthesis of WC from WO3 and carbon black [128] 21
Figure 7: Schematic of the CVD Process [135] 23
Figure 8: Synthesis of WC and molybdenum carbide composite [143]. 26
Figure 9:Polarization curves of the prepared samples for OER (b) Tafel slope of the corresponding samples for OER [145]. 27
Figure 10:(a) Polarization curves of different materials for HER. (b) corresponding polarization curves for OER [146]. 27
Figure 11: a) LSV polarization curves of OER, (b) the corresponding Tafel plots for OER, (c) LSV polarization curves (d) the corresponding Tafel plots [148]. 29
Figure 12:Cyclic voltammetry curves for (a) platinum and (b) tungsten carbide cathodes in molten CsH2PO4 at increasing temperatures [152]. 29
Figure 13: Process Flow of the Method Used for the Preparation of Catalyst. 33
Figure 14:XRD of the (a) Pure WC, (b) Pure PBNPs, (c) Pure UiO-66, (d) Hybrids. 37
Figure 15: (a-i) SEM images of all the prepared hybrids and pure samples (J, k) EDX of WC 4 and WC 3. 41
Figure 16:(a, b) LSV curves for HER, (c, d) LSV curves for OER. (e, f) Tafel plots of HER, (g, h) Tafel Plots of OER. 47
Figure 17:(a) CVs of WC@PBNPs hybrids (b) CVs of WC@UiO-66 hybrids (c) CV curves of WC 6 at different scan rates, (d, e) TOF of the hybrids for HER, (f, g) TOF of Hybrids for OER. 49
Figure 18:(a, b) EIS of the prepared samples, (c) Chronopotentiometry of WC 6. 52

List of Tables

Table 1: Properties of WC [51].....4
Table 2: Comparison of different electrocatalyst.....13
Table 3: Electrochemical Water Splitting Performance of WC and its Hybrid for HER and OER.....30
Table 4: crystal Size and peak position and FWHM of the prepared samples. 37
Table 5: Comparison of some catalyst with this research.....44
Table 6: Resistance and ECSA of the prepared samples. 51

Acronym

TOF: Turnover Frequency

MOF: Metallic Organic framework

FE: Faradaic Efficiency

OER: Oxygen evolution reaction

HER: Hydrogen evolution reaction

WC: Tungsten Carbide

PBNPs: Prussian blue

UiO-66: Zirconium based MOF.

ECSA: Electrochemical active surface area

SEM: Scanning Electron Microscope

EDX: Energy-dispersive X-ray spectroscopy

FTIR: Fourier-Transform Infrared Spectroscopy

XRD: X-ray diffraction

Oxidation: Ox

Reduction: Red

dec^{-1}: Decade

Pt: Platinum

CV: Cyclic Voltammetry

LSV: Linear Sweep Voltammetry

EIS: Electrochemical Impedance Spectroscopy

Chapter 1

Introduction

1.1 Background

As the population of the world is increasing at a rapid rate, it results in the use of more energy. According to research, a 26% increase in the world population will occur by the end of 2050, and with this increase, the usage of the world's primary energy will also be increased by a factor of 50% [1, 2]. This increase in world energy usage is leading the way towards the depletion of the energy reservoirs, i.e., oil reservoirs, gas reservoirs, and fossil fuels [3-5]. In a report published by the international energy agency, the estimated usage of energy can reach up to 13.371 billion tons of oil (btoe) in 2012, and by the year 2035, it will reach 18.30 btoe representing a growth of 1.37% [6]. The use of fossil fuels also gave rise to many problems like global warming, as carbon dioxide CO_2 is produced as a result of the use of fossil fuels, and it is the primary contender of green house effect and is the most dangerous greenhouse gas as its lifetime is too large, along with these other problems are water contamination, air pollution and many more [7-10]. So, if this issue is not addressed properly, by the end of 2052 the overall temperature of the earth could rise by 1.5 ^{0}C [1, 11]. Because of these issues, scientists tried to find an alternate way of producing energy that is (a) green with no carbon emission (not harmful to our environment) (b) sustainable, and, (c) renewable [12]. This alternative way of energy will reduce the use of fossil fuels by providing the same amount of energy, and reduce the emission of CO_2 will also be reduced to a greater extent [13]. Among all the proposed solutions for the given problem, the best one is the production of hydrogen for energy purposes, as it fulfills all the criteria for green energy [14-16]. Hydrogen fuel can be produced from renewable sources. As a result, its life cycle is also clean and renewable [17-19]. It is a carbon-neutral and highly efficient source of energy because of its high energy storage capacity. The energy density of hydrogen makes it a potential alternative to carbon-based fuels. In addition to these benefits, hydrogen is used to power pollution-free autos, as a household fuel, and for aircraft propulsion [20, 21]. Hydrogen can be produced mainly through 3 techniques, i.e. (a) Steam Methane Reforming (In the presence of steam Methane is

converted into hydrogen gas and carbon dioxide), (b) Coal Gasification (Here coal is used instead of methane to produce the same products i.e., H_2 and CO_2 in the presence of steam), and (c) Water Electrolysis (Here water in the presence of electricity and catalyst is converted into hydrogen and oxygen. **Figure 1** shows all three methods for hydrogen production. Among the anticipated techniques mentioned, the electrochemical method is the best technique in terms of the cleanness and efficiency of hydrogen production. Presently hydrogen is mainly produced from fossil fuels, about 95% and the remaining 4% of hydrogen is taken from renewable resources i.e., electrochemical study (water electrolysis) [22-24]. As currently most of the need of energy is fulfilled from fossil fuel and in the result CO_2 is produced along with hydrogen and with-it fossil fuel are going toward depletion. So, the best alternative method left behind is that of water splitting method for the production of hydrogen with zero carbon emission [4].

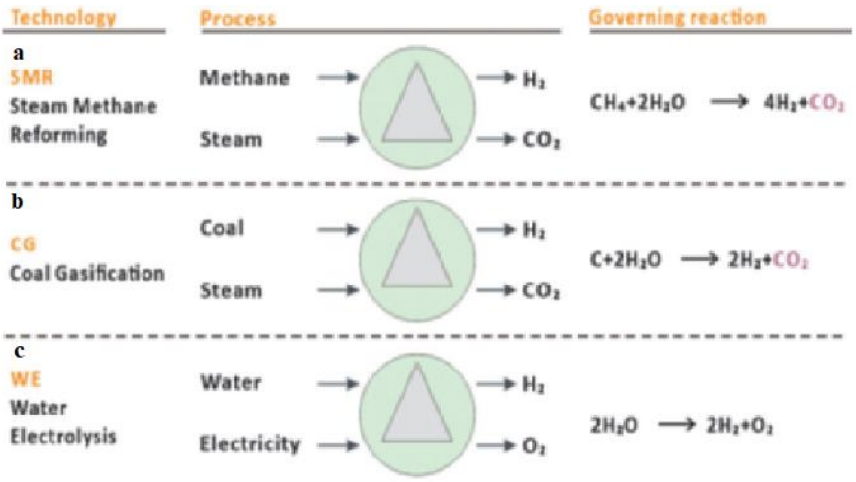

Figure 1: (a) Steam Methane Reforming (b) Coal gasification (c) Water Electrolysis [22]

Water splitting is basically the breaking of a water molecule into hydrogen and oxygen with the help of a catalyst [25, 26]. Because only water is used as raw material and the products are hydrogen and oxygen, this process is environmentally friendly as no carbon is produced in the meantime [27-29]. Besides this, oxygen produced is also used in different industries, so it increases the economic probability of the electrolysis process. Diverse approaches exist for separating water.

(a) Photocatalytic water splitting, which uses visible light and a photocatalyst to divide water [30-32].

(b) Electrochemical water splitting: In this method, an electrocatalyst is utilized to split water into its constituents, hydrogen and oxygen, utilizing electricity [33-36].

(c) Photobiological water splitting occurs with the aid of an algae bioreactor; the yield of hydrogen production is decreased utilizing this method [37-39].

(d) Radiolysis, the major drawback with this method is that nuclear wastes are produced at the end [40].

The thermodynamics of water splitting shows that the reaction is a multi-electron process and endothermic reaction [41]. As the reaction is endothermic so it will require a certain amount of energy to fulfill the Gibbs free energy change (ΔH^0 = 238 KJ mol $^{-1}$) [42]. Hydrogen production from water simply requires 2.458 eV of energy which is an alternative to a potential difference of 1.22 V for the displacement of 2 electrons, and as 4 electrons are needed to produce two moles of hydrogen, so 4.915 eV of energy is required in whole [43]. Water splitting involves two half-reactions: hydrogen evolution reaction (HER), in which reduction of protons occurs to produce hydrogen, i.e., H_2, and the oxygen evolution reaction (OER); in this reaction, oxidation of water takes place to form oxygen gas [44]. The kinetics of both these reactions shows that the reactions are not favored without a catalyst. To carry the reactions feasibly, there is a need to find a suitable catalyst that overcomes the energy barrier and speeds up the overall water-splitting reaction. In this regard, Pt catalyst is used most often for hydrogen evolution reaction while Ir/Ru based compounds are used as a benchmark for oxygen evolution reaction. But due to the high cost and limited availability of these noble metals, the process of water splitting cannot be applied on an industrial scale. Due to these reasons, a catalyst for the process is needed, which is not only readily available but also exhibits high catalytic activity and stability. Transition metals sulfides, carbides, and phosphides are the good competitors having all the required properties of a good catalyst for HER, and transition metals phosphate, oxides, and hydroxides are among the good catalysts for OER [45].

Among the catalysts, tungsten carbide WC is the best catalyst for hydrogen production by providing a low Tafel slope and low overpotential compared to other catalysts. WC is a material made by the covalent bond of tungsten and carbon atoms having good strength and melting point. The use of tungsten carbide in place of Pt in water splitting shows promising results as it provides? the same efficiency by reducing the cost [46]. The catalytic activity of tungsten carbide depends on the method of preparation, the raw materials used, and the reaction temperatures [47]. Tungsten carbide usually exists in two forms, i.e., tungsten carbide (WC) and tungsten dicarbide (W_2C). Both of these forms synthesize simultaneously in the synthesis of carbide [48]. The crystal lattice of WC is hexagonal, and that of W_2C is orthorhombic [49], and in these two forms, WC shows lover Tafel slope and overpotential as compared to W_2C [50]. The physical, chemical and mechanical properties of tungsten carbide are presented in Table 1 [51].

Table 1: *Properties of WC [51]*

Property	**Value Range**	**Units**
Poisson's Ratio	0.2-0.22	-
Young's Modulus	600-686	GPa
Density	15.25-15.88	g/cm^3
Hardness	17.0-36.0	GPa
Melting Point	2,727-2,920	°C
Compressive Strength	3.35-6.83	GPa

Despite these properties, pure WC has strong adsorption for H due to which it shows low activity for hydrogen evolution reaction in alkaline media [52]. So, to enhance the HER activity of tungsten carbide some modification must be done. The best way to do it is to make hybrids of WC with MOFs [53].

Prussian blue (PBNPs) is a metal-organic framework with Fe as a central atom connected to ligands discovered recently is used for the preparation of various hybrids because of its properties. Due to its large surface area and metal active sites, hydrogen intermediates are

adsorbed and converted to hydrogen molecules (H_2) [54]. In PBNPs iron is present in the +2-oxidation state with carbon and +3 oxidation state with nitrogen due to this quality electron transfer to the conduction band is very fast [54-56]. Some of the fascinating properties of these PB complexes include their solubility, stability, porosity, low density, flexible molecular structure, and variable physical and chemical properties [56].

UiO-66 is also a MOF of Zr central atom with benzene 1-4 dicarboxylic acid as the organic ligands. The crystal structure of UiO-66 is in the form of an octahedron which possesses large surface area. Moreover, UiO-66 has high mechanical, electrical, and chemical stabilities [57]. Formation of high charge density and polarization takes place because of the strong bonding of the carboxylate O atom and Zr (IV) atom. With such properties, UiO-66 is one of the promising candidate for the water splitting technique [58]. As the electron transfer in any catalyst is strongly dependent on the crystalline nature of the catalyst so MOF always finds itself a suitable candidate for it because of the presence of metal as a center atom [59, 60].

Keeping this literature in mind that tungsten carbide will enhance its catalytic activity with MOFs we synthesize hybrids of WC with Prussian blue PBNPs and UiO-66 MOFs and study its electrochemical behavior. The synthesis route of pure tungsten carbide by the solid-gas reaction is discussed along with the hybrid synthesis by hydrothermal for UiO-66 and the sonication method for PBNPs. The electrochemical result shows the better activity of hybrids compared to that of the pure catalyst. This enhanced activity of the hybrids is purely due to the structure modification, increased surface, and synergistic effects of both the material in the hybrid.

1.2 Electrochemical water splitting (Fundamental Aspects):

As shown in **Figure 2,** in electrochemical water splitting, the electrolyzer is composed of three parts the electrolyte, the anode, and the cathode. Catalyst is used on the surface of the cathode and anode to enhance the overall reaction of the water splitting. The reaction starts when voltage is applied from an external source. The HER reaction takes place at the

cathode, producing hydrogen gas and the OER reaction occurs at the anode, and the final product, in this case, is the oxygen gas. The overall reaction to water splitting is

$$H_2O \rightarrow H_2 + \frac{1}{2}O_2$$

In acidic media, this reaction is

$$\text{At cathode } 2H^+ + 2e^- \rightarrow H_2$$

$$\text{At Anode } H_2O \rightarrow 2H^+ + 1/2O_2 + 2e^-$$

In neutral solution

$$\text{At Cathode } 2H_2O + 2e^- \rightarrow H_2 + 2OH^-$$

$$\text{At Anode } 2OH^- \rightarrow H_2O + 1/2O_2 + 2e^-$$

Water electrolysis is classified into 4 different categories based on the type of electrolyte used they are (a) Alkaline water electrolysis [61-64] (b) microbial cell electrolysis (c) solid oxide electrolysis [62, 65, 66] (d) PEM water electrolysis [62, 67, 68].

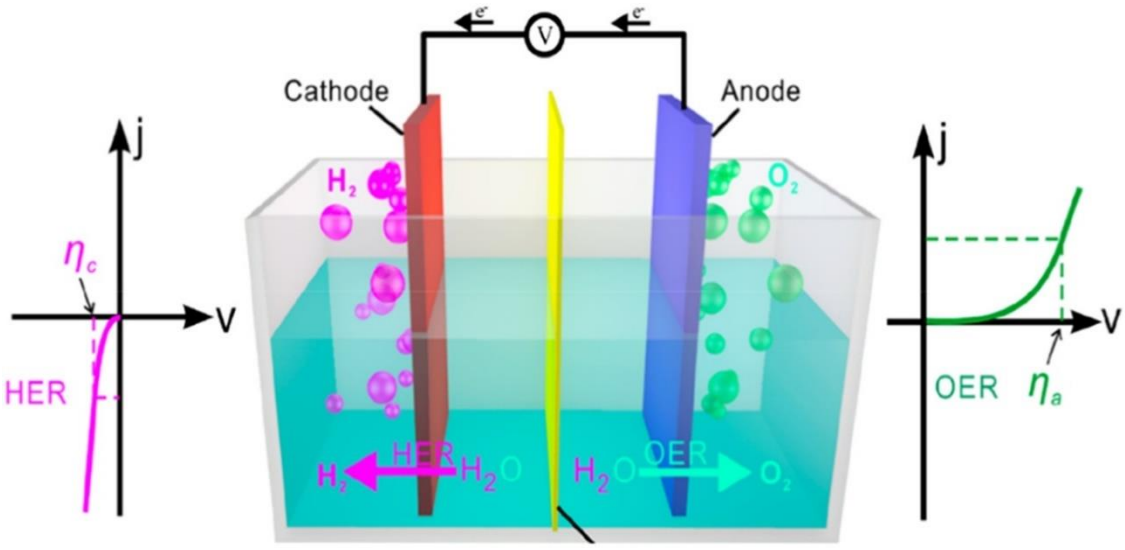

Figure 2: HER and OER reactions of water splitting [69]

In 1789 Troostwijk and Diemann jointly introduced the phenomena of alkaline water electrolysis [23, 62, 69-71]. In this process, two molecules of alkaline nature, i.e., potassium hydroxide and sodium hydroxide, are reduced to hydrogen H_2 molecule and

hydroxyl ion at the cathode. The H_2 produced eliminates from the cathode and released in the form of gas. The OH ion move toward the anode under the sway of an electric charge. At the anode, it splits into ½ of O_2 and one molecule of water [23, 63, 72]. In 2005 Penn state university and Wageningen University, two research organizations introduced a new novel electrolysis technique in which organic matter was used and called microbial electrolysis cell [23, 73-75]. During this process, first, the substrate was oxidized into CO_2, proton, and electrons at the anode. With the help of an electric circuit, these protons and electrons move towards the cathode through electrolyte and external circuits respectively, and combined there to produce hydrogen [23, 74]. In comparison to water electrolysis, microbial electrolysis cell requires a small amount of external energy as well. In 1980, Donitz and Erdle introduced solid oxide electrolysis, a method for efficiently producing pure hydrogen Compared to other electrolysis procedures, the temperature and pressure of this process are substantially elevated [76, 77]. This method utilizes water as steam and O_2 conductors that are typically derived from nickel/yttria-stabilized zirconia. [78]. In 1966 Grubb discovered proton exchange membrane electrolysis to cover the short coming of alkaline water electrolysis. Some of the merits of using the proton exchange membrane are high proton conductivity, low thickness, and high-pressure operations. Catalysts used for PEM electrolysis are Pt for HER at the cathode and IrO_2/RuO_2 at the anode for OER [77, 79, 80]. The basic principle of water splitting is the same for all the categories and involves two reactions, i.e., hydrogen evolution reaction HER and oxygen evolution reaction OER.

1.3 Hydrogen Evolution Reaction (HER):

As the kinetics of HER is comparatively simple, therefore it is the most studied electrochemical reaction of water splitting. HER reaction has been explored for all the transition metals. HER is the combination of three chemical reactions (3 steps) that is adsorption, chemical, and electrochemical desorption. These three reactions are named 1: Volmer reaction, 2: Heyrovsky reaction, and 3: Tafel reaction [23, 81-83]. Basically, HER is two electron transfer mechanism which is initiated by Volmer reaction. The mechanism is different for acidic and alkaline medium. For acidic medium intermediate of hydrogen (H^*) is formed by the evolution of a hydronium ion that are absorbed on electrode surface while in case of alkaline medium it is the water molecules that act as proton source. So,

hydrogen molecule is produced using two different ways which strongly depend on the surface coverage of hydrogen intermediate. If this surface coverage of the intermediate is high, then Tafel step will be the rate limiting step in which two adjacent intermediate combine and form a molecule of hydrogen. When the coverage is low then the rate limiting step is the Heyrovsky reaction in which a single intermediate will attract the proton and electron in acidic medium and electron and water molecule in the basic medium [84-86]. Water splitting usually takes place when the energy given is high enough to overcome the over potential and losses [87].

Volmer reaction:

$$H_2O + M + e^- \rightarrow MH_{ads} + OH^- \text{ (In alkaline medium)}$$

$$H^+ + M + e^- \rightarrow MH_{ads} \text{ (In acidic medium)}$$

Heyrovsky reaction:

$$MH_{ads} + H_2O + e^- \rightarrow M + OH^- + H_2 \text{ (In alkaline medium)}$$

$$MH_{ads} + H^+ + e^- \rightarrow M + H_2 \text{ (In acidic medium)}$$

Tafel reaction:

$$2MH_{ads} \rightarrow 2M + H_2$$

The free energy of hydrogen adsorption depends on the catalyst. The free energy of a good catalyst must be close to zero. This is because of the low adsorption, which leads the way toward the poor interaction of the proton and electrode surface. If the free energy is high, then it will be difficult to break the bond between a catalyst surface and hydrogen [85, 88, 89].

1.4 Oxygen Evolution Reaction (OER):

Oxygen evolution reaction is also a four-electrode process. Here also, the mechanism of the reaction is different for acidic and alkaline solutions. For acidic media, oxidation of water takes place to produce oxygen gas and hydrogen gas. On the other hand, in alkaline media, it is the hydroxyl ion that oxidizes into water and oxygen. The overall mechanism of both types of media is discussed as

For acidic media,

$$H_2O + \bullet \rightarrow HO^{\bullet} + H^+ + e^-$$

$$HO^{\bullet} \rightarrow O^{\bullet} + H^+ + e^-$$

$$O^{\bullet} + H_2O \rightarrow HOO^{\bullet} + H^+ + e^-$$

$$HOO^{\bullet} \rightarrow \bullet + O_2 + H^+ + e^-$$

In basic media, the reactions are

$$OH^- + \bullet \rightarrow HO^{\bullet} + e^-$$

$$HO^{\bullet} + OH^- \rightarrow O^{\bullet} + H_2O + e^-$$

$$O^{\bullet} + OH^- \rightarrow HOO^- + e^-$$

$$HOO^{\bullet} + OH^- \rightarrow \bullet + O_2 + H_2O + e^-$$

Here • signify the active surface area of a catalyst. Here in the oxygen evolution reaction, the potential determining step is the step that possesses a high energy hindrance. The free energy of an ideal catalyst is seen to be 1.23 eV [85].

1.5 Key Performance Indicators (KPI):

The evaluation parameter for water splitting is the catalyst activity which can be determined from certain key parameters like Tafel slope and overpotential. Besides this, available active sites are also the key factor of an electrocatalyst which can be enhanced through the formation of high surface area structures, making nanostructures, and making changes in the morphology [90]. Tafel slope is a plot that correlates reaction rate with the overpotential. For an ideal catalyst, it is necessary to have a low Tafel slope and high current density [85]. Tafel slope is related to the current density logarithmically by the following relation

$$\eta = a + b \log (j/j_0)$$

In this equation, η is the overpotential, b is the Tafel slope, j is the current density, j_o is the exchange current density [91-93], and it is obtained when the overpotential is taken as zero, and basically, it's the intrinsic catalytic activity of an electrode under equilibrium condition.

Actually, a good catalyst has a high j_o and a low Tafel slope (b). Overpotential is another parameter for determining catalyst activity. Overpotential is the extra potential that is required to start the reaction of the catalyst, whether it is for HER or OER. The value of overpotential is always greater than the equilibrium potential. For an ideal catalyst, the overpotential is low, so the lower the overpotential of a catalyst, the better that catalyst will be and the higher the electrochemical activity of the catalyst will be. The stability of a catalyst is another important parameter in the evaluation of a catalyst in the production of hydrogen. The stability of a catalyst can be measured using two methods, i.e., galvanometric/potentiostatic electrolysis and CV (repetitive cyclic voltammetry or LSV (linear sweep voltammetry. In CV and LSV, change in over potential after certain cycles indicate the stability of the whole electrolysis process, whereas, in the other method, changes in the potential with respect to time are monitored at constant current density[94]. Another key parameter in catalytic water splitting is the faradaic efficiency. It is the number of electrons that participated in the hydrogen evolution reaction that is provided by an external circuit.The catalytic rate of a catalyst was first proposed by Michel Boudart in 1968 in terms of turnover frequency (TOF). It is the number of molecules that are reacting per site in one second [95]. It is one of the important KPIs in electrochemical water splitting. TOF can also be defined as the number of molecules that are taking part in a reaction and transformed to desired product per site in unit time [96]. Due to the non-uniform availability of the active sites of different catalysts, it is quite difficult to find out the turnover frequency of some catalysts. It is normally calculated by using the given equation $TOF = \frac{jA}{4nF}$. In this equation, A is the working electrode area, and n is the number of moles of active material [97, 98].

1.6 Problem Statement

The demand and use of energy are increasing day by day and the only source of energy in the past was the natural resources i.e., oil and natural gas but with time these resources are depleted so researchers find an alternative for it in the shape of hydrogen which is a clean and pollution free source of energy. Hydrogen can be produced through many techniques like catalytic water reforming from methane and water splitting technique. Water splitting is used to produce H_2 in the presence of a catalyst. At first noble metal like Pt was used as

a catalyst for this purpose but as they are more expensive and going to be depleted therefore there is a need to synthesize such catalyst which enhance the kinetics of the reaction and is less costly. In this research WC based hybrids will be used as a catalyst to produce hydrogen gas. The method of electrochemical water splitting will be used in this research which is the splitting of water through electrolysis.

1.7 Research Objective

The research objective is as follow

- Synthesis and characterization of WC hybrids
- Lowering the overpotential of prepared hybrids
- Application of hybrids for HER (hydrogen evolution reaction) to see catalytic performance.

1.8 Scope of Study

As Pakistan is a developing country and it has lack of many resources in form of energy so hydrogen production will cover that deficiency of energy because we can use that hydrogen as a fuel and in electricity and many more.

- One of the best advantages is that hydrogen produced in this process is renewable and as water is used which is the most abundant in nature so there is no problem of depletion of water. Moreover, the use of transition metals as a catalyst will reduce the use of precious noble metal and prevent it from depletion.
- Hydrogen produced in the process of water splitting has many applications like it can be used as a domestic fuel, it can be used in vehicles, it can also be used as a raw material for many chemicals like ammonia etc.

1.9 Chapter Summary

This thesis consists of 5 chapters. The acquaintance of each chapter is given in the following chapters.

- **Chapter 1** delivers vision of the subject, background and contemporary problems related to the work. It also clarifies the problem statement, research objectives and scope of the planned study.
- **Chapter 2** will sketch the literature review achieved to describe the previous work done on the synthesis of WC hybrids, previous method technique, water splitting and its factors. It also includes review based to compare WC based hybrids with different hybrid electrocatalysts.
- **Chapter 3** covers the methodology related to the synthesis of pure WC, pure PBNPs, pure UiO-66 and hybrids.
- **Chapter 4** elaborate the result and discussion. The analysis of XRD and SEM to describe the phase of crystal structures and morphology of the synthesized catalysts. The chapter also elaborate Electrochemical studies of the active catalysts and its stability.
- **Chapter 5** reviews all the findings and conclusions in the current study and provides the future recommendation for the related work.

Chapter 2

Literature Study

2.1 Literature Review:

A lot of research has been carried out on the water splitting process for the production of hydrogen because of the depletion of the energy reservoirs. Transition metal carbides sulfides and phosphides gain immediate attention because of its platinum like properties. Among these transition metal the metals of carbides have been studied because it possesses exceptional electrocatalytic activity. In this regard many researchers studied WC and shows that WC has Pt like behavior in both alkaline as well as acidic electrolytes. Further it is noticed that the electrocatalytic activity can be enhanced by making hybrids of WC with different metal organic framework. this enhancement in the activity is because of the synergistic effects of the material present in the hybrids. Some of the previous work done on tungsten carbon and its hybrids are given in table 2.

Table 2: Comparison of different electrocatalyst

Catalyst	Synthesis Method	Reaction type	Over potential (mV)	Tafel slope(mV/dec)	Current density (mA/cm^2)	Electro lyte	Ref
Ni-WC	Hydrothermal method	OER	130	75	10	0.5 M H_2SO_4	[99]
WC-Nikle doping	Electro spinning followed by calcination	OER	378	93	10	1 M KOH	[100]
Ni_2-W_4C-W_3C/ CNFs	CVD Process	HER	63	112	10	1M KOH	[101]
Ni_2-W_4C-W_3C/ CNFs	CVD Process	OER	270	52	30	1 M KOH	[101]
W_6Co_6C @NC	Solid gas Reaction	HER	59	45	10	1 M KOH	[102]

W_6Co_6C @NC	Solid gas Reaction	OER	286	54	10	1 M KHO	[102]
Mo-WC/NCS	Sample Mixing followed by Solid Gas Reaction	HER	179	81	10	Acidic or neutral media	[103]
W_2C-HS	Solvo thermal Process	HER	153	67.8	10	0.5 H_2SO_4	[104]
$W_{1-x}Ni_xC$ NCs/NF	Hydrothermal Method	HER	190	102	10	Alkaline Solution	[105]
$W_{1-x}Ni_xC$ NCs/NF	Hydrothermal Method	HER	148	81	10	Acidic Solution	[105]
WC@NPC	Pyrolysis Method	HER	51	49	10	0.5 H_2SO_4	[106]
H-WC	Solid Gas Synthesis	HER	160	102	10	0.5 H_2SO_4	[107]
B-WC	Solid Gas Synthesis	HER	313	138	10	0.5 H_2SO_4	[107]
W_2C-NC-WN	Solid Gas Reaction	HER	145	96	10	1 M KOH	[108]
W_2C	Hydrothermal Process	HER	274	145	10	0.5 H_2SO_4	[109]
2 % Fe-W_2C	Hydrothermal Process	HER	197	102	10	0.5 H_2SO_4	[109]
2% Co-W_2C	Hydrothermal Process	HER	157	122	10	0.5 H_2SO_4	[109]
2% Ni-W_2C	Hydrothermal Process	HER	57	39	10	0.5 H_2SO_4	[109]
WN- W_2C	Solid Gas Synthesis	HER	242	85	10	0.5 H_2SO_4	[110]
P-WCx NWs/CC	-	HER	118	55	10	0.5 H_2SO_4	[111]
P-WCx NWs/CC	-	HER	122	56	10	1 M KOH	[111]

Co-WC/CN	Solid Gas Reaction	HER	98	-	10	1M KOH	[112]
i-WC- G	Solid Gas Reaction	HER	120	38	10	0.5 H_2SO_4	[113]
α-W_2C/WN @G	Solid State Reaction	HER	120	69	10	0.5 H_2SO_4	[114]
MoS_2/WC /RGO	Solvothermal Method	HER	200	41	10	0.5 H_2SO_4	[115]

2.2 Synthesis of Pure Phase WC:

There are different methods for the synthesis of tungsten carbide with different results in the final product. They are discussed here one by one.

2.3 Hydrothermal method:

In a typical synthesis of tungsten carbide (WC), 5 gm of AMT, i.e., Ammonium Meta Tungstate, was dissolved in hot deionized water, and 4.6 gm of corn starch was added to the above solution, and the solution is well-mixed. This solution was transferred to a Teflon-lined autoclave and placed in the oven for 8 hr at 200^oC. After 8 hr, the solution was taken out and dried at 250^oC by using the spray drying technique. In the end, the product was obtained by calcining the precursor for 1 hr in a vacuum furnace at 980^oC [46]. In another synthesis, WC was hydrothermally prepared from WO_3 precursor in this method, 0.6597 gm of sodium tungstate dihydrate ($Na_2WO_4.2H_2O$) and 0.5286g of ammonium sulfate $(NH_4)_2SO_4$ was dissolved in 15ml of deionized water. After the solution was thoroughly mixed, 3M HCl was added solution to maintain the PH of the solution at 2. Then the solution was poured into a Teflon-lined stainless autoclave and started the reaction at 180^oC for 8 hr in the oven. After the reaction time was completed, the precursor was washed with water and ethanol three times and then dried at 60^oC. Then prepared, WO_3 was taken and mixed with glucose with a molar ratio of W/C = 0.078 in deionized water and stirred for 20 min. After this, the solution was transferred to a Teflon-lined autoclave and heated in the oven at 180^oC for 8 hr to form carbon-coated tungsten oxide nanorods. In the end, the prepared precursor was calcined in a tube furnace in H_2/Ar media

(V_{H2}/V_{Ar} = 1:3) at 900°C for 3 hr Schematic is shown in **Figure-3** [116]. J. Bernard d'Arbigny et al. synthesized WC from ammonium meta tungstate (AMT) and glucose by varying the ratio of AMT/glucose from 1.10^{-2} to 1.11^{-1}. In this method, a blend of AMT and glucose was made by mixing in deionized water, and the blend was poured into a Teflon-lined autoclave and heated at 170°C for 12 h in an oven. Then at the completion of the reaction, the precursor was dried overnight at 70°C. Then the prepared precursor was heated at 900°C for 2 hr using Argon as a medium. To methanise, the free carbon heat treatment of the product is done in a hydrogen medium from 20°C to 900°C [117]. Leyan Xiong et al. also used ammonium meta tungstate AMT and glucose in different ratios and mixed it in deionized water to make it a transparent solution. The solution was then poured into a Teflon-lined autoclave and heated at 180°C for 12 h. Then the solution was dried at 100°C for 3 hr, and at the end, the prepared precursor was calcined at different temperatures in a tube furnace in hydrogen media to get WC nanopowder [118].

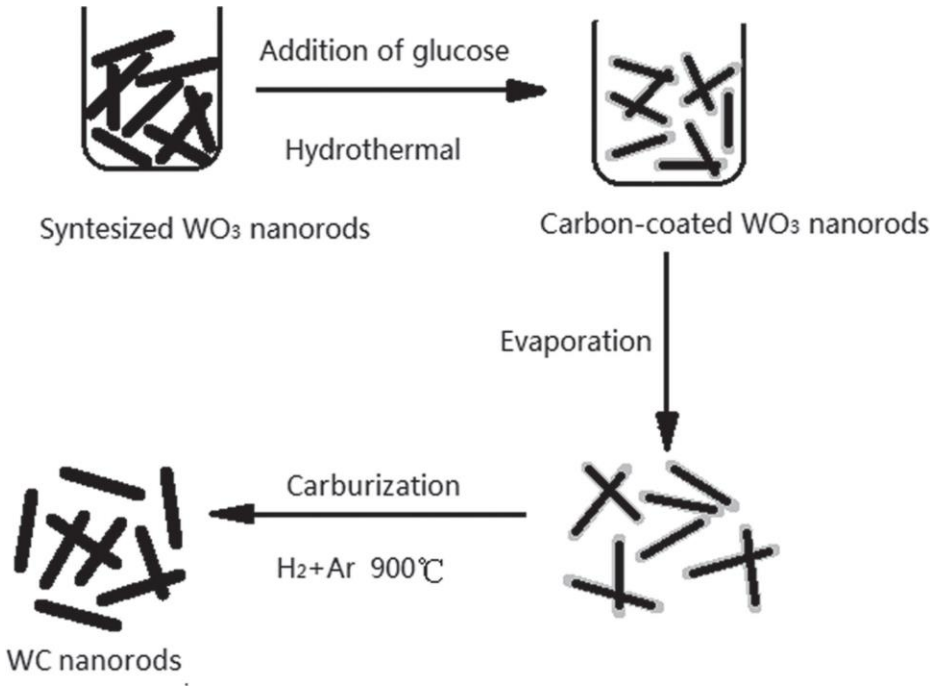

Figure 3: Synthesis of WC from WO3 precursors [118]

Yi Wang et al. used the hydrothermal method. In his method, he dissolved 4g of cetyltrimethylammonium bromide (CTAB) in 20 ml of deionized water, and the solution

was stirred for 20 minutes. Then he poured this solution into another solution of 20 ml containing a different molar ratio of AMT and glucose. The resulted solution was then treated hydrothermally at 180^{o}C for 24 hr in a sealed Teflon-lined autoclave to prepare the precursor. In the end, the precursor was calcined at 900^{o}C under H_2/N_2 flow (VH_2/VN_2 = 1:3) for 60 minutes to 240 minutes to get the final product, i.e., Nanochain-structured mesoporous tungsten carbide [119]. Gopal Boopathy et al. took 5 g of ammonium meta tungstate AMT and dissolved it in hot deionized water and added 4.6 g fructose to the solution. After proper mixing, the solution was transferred to a Teflon-lined autoclave and heated for 12 h at 220^{o}C. After the completion of the reaction, the precursor was dried using the spray-dried technique at 250^{o}C. To get the final product, i.e., WC, the precursor was heated at 900^{o}C for 2 hr in a vacuum furnace Schematic is shown in **Figure 4** [120]. Yi Wang et al. synthesized WC by using a simple hydrothermal method. First, a transparent solution was prepared by dissolving AMT and glucose in deionized water. The molar ratio of glucose to AMT was 100:1. The solution was then heated at the rate of 5^{o}C min^{-1} in a Teflon-lined autoclave for 12 h; the end temperature was 170^{o}C. The precursor was then washed several times with ethanol and deionized water and, in the end, dried at 70^{o}C in a vacuum oven. The prepared sample was then calcinated at 950^{o}C in pure Argon media in the quartz tube and then carbonized at 950^{o}C in argon flow for 2 hr. Finally, free carbon was removed from the prepared product by heating it at the same temperature in a hydrogen medium. The Schematic is shown in **Figure 5** [121]. Jing Gao et al. took 13.2 g of sodium tungstate hydrate ($Na_2WO_4 \cdot 2H_2O$) and dissolved it in 500ml deionized water. After mixing, 2 mol dm^{-3} of HCl

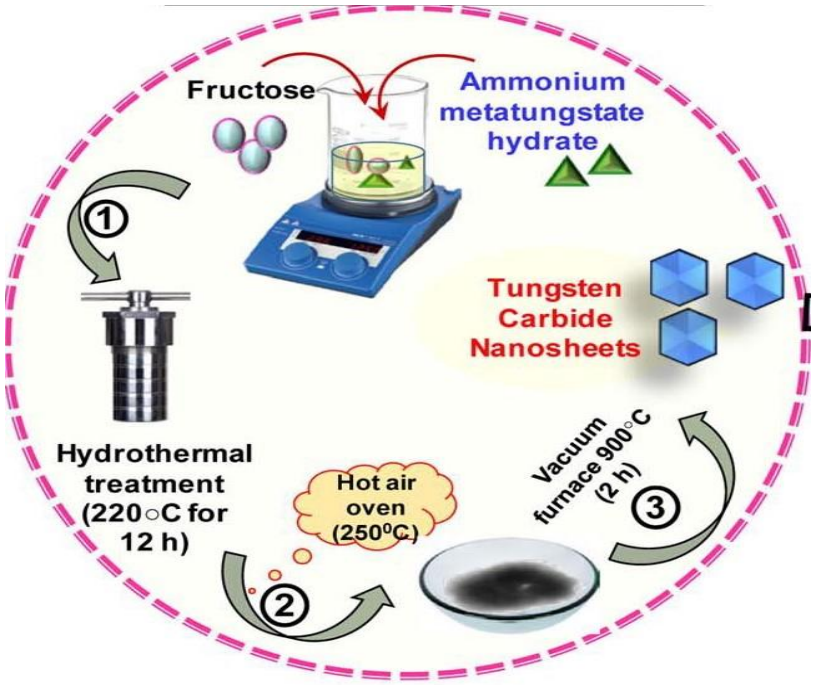

Figure 4: Synthesis of WC Nanosheets From Fructose and AMT[122]

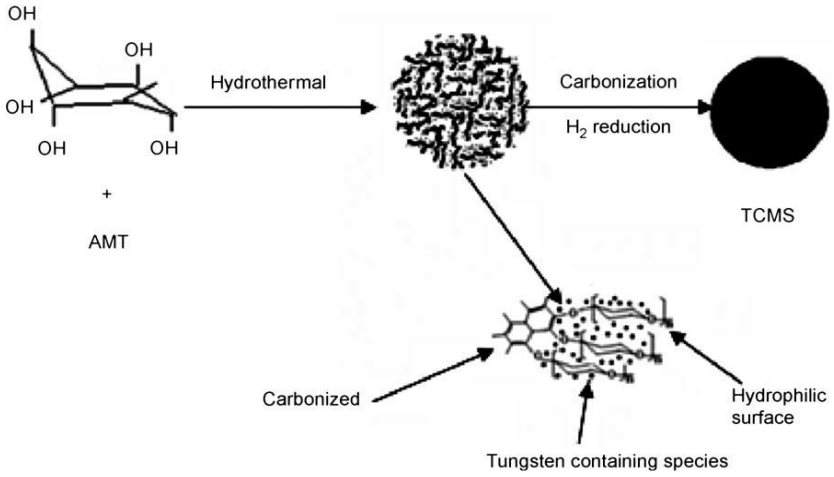

Figure 5: Synthesis of WC from AMT and Glucose [123]

solution was added to it dropwise and maintained the pH of the mixture to 1. Then 1 g oxalic acid was added to the mixture and stirred for 30 minutes. Then the solution was transferred to a hydrothermal reactor and put on a stove, raised the stove temperature to 100^{o}C at a rate of 10^{o}C/min, and kept at this desired temperature for approximately 4 hr. After the completion of the reaction, the reactor was cooled to atmospheric temperature.

The precursor was washed with deionized water and ethanol and then dried at 60^{o}C for 24 hr. Now 10 g of the prepared precursor was taken in a quartz boat and transferred to a tube stove, and keep it under N_2 flow for 30 min to remove all the air. Then he started heating the precursor at 10^{o}C/min and rising up to the final temperature of 650^{o}C for 6 hr under hydrogen (H_2) and methane (CH_4) flow; the ratio of H_2 to CH_4 was 2:3. Then the product was cooled at room temperature for further use [122].

2.2.2 Solid-State Reaction:

F.F.P. Medeiros et al. synthesized tungsten carbide (WC) using a solid-gas reaction. In this typical synthesis, Ammonium Para tungstate APT and tungsten blue oxide TBO were used as tungsten sources. 3 g of APT or TBO was taken in a boat and put in the reactor and heated for 2 hr at a rate of 5^{o}C/min up to 850^{o}C under CH_4 + H_2 flow. The flow of the CH_4 + H_2 was 20l/min [123]. J.Ma et al. synthesized tungsten carbide using graphite and WO_3 precursors. Stoichiometric amounts of both the chemicals were mixed in a ball mill in argon media for 10 hr. The powder to ball weight ratio was 1:10, and the speed of the mill was 350 rpm. After 10 hr, the sample was transferred to a boat and heated in a furnace at 1215^{o}C for 1 hr. The temperature gradient during the reaction was 10^{o}C/min [124]. Monsur Islam et al. mixed Iota-carrageenan (IC) with chitin in a weight ratio of 1:4. After proper mixing, he added WO_3 to the mixture and kept the ratio of WO_3/C 1:6, and vortexed for 10 min. Once the biopolymer was mixed properly, he took 5 g of this mixture and dissolved it in 15 ml of pure water using a spatula. A gel-like solution was formed named polymer composite precursor (PCP). The PCP was heated at various temperatures under nitrogen gas flow to get the required product of WC [125]. Kai-Fei Wang et al. synthesized WC by mixing WO_3 and carbon black with different molar ratios (2.7, 2.9, 3.1, 3.5, and 3.7) in an agitated motor for 20 min. Then 10 g of the mixed powder was poured into the alumina boat, which was accommodated in a constant temperature zone. The sample was then heated to the desired temperature and kept under the protection of Argon flow. The heating rate was 5^{o}C/ min. The sample was cooled at the rate of -10^{o}C/min before the removal of the sample from the furnace. The prepared mixture was kept inside a constant temperature zone, and the temperature of the furnace was raised to the required values at a heating rate of 5^{o}C min^{-1}. In order to initiate the calcination process, the mixture was kept for 6 hr under

a hydrogen flow rate of 100 ml min^{-1}. The Schematic is shown in **Figure 6** [126]. Angel T. Garcia-Esparza et al. prepared tungsten carbide nano rods from tungsten chloride WCl_6 and ethanol. In the typical synthesis, WCl_6 was dissolved in ethanol. The metal precursor reacted rapidly and formed HCl and a stable precursor of metal–ortho ester. Sonication of the precursor was done to increase the rate of solubilization. 0.5 g mpg-C_3N_4 was added by drop impregnation type process to maintain the weight ratio of precursor compound at 1:1. In the end, the finally synthesized precursor was put in an alumina boat and heated from 1073K to 1373K under nitrogen flow to obtain the final product [127]. Rasit Koc et al. took WO_3 as a source of tungsten and carbon black as a source of carbon. A split furnace was used for the preparation of precursor gas. This furnace is used to prepare a carbon-coated WO_3 gas using propylene as a coating gas. In its typical synthesis, 200 g of the precursor is placed in the furnace, and the vessel is purged with Argon and then heat the furnace to 600^oC. When the temperature reached this value, it was kept at this temperature for 30 min. Then the vessel was filled with propylene gas, and the sample was kept under the pressure of 3-5 atm for 5-20 min. Thermal carking of propylene increased the pressure inside. The residual gas was discharged, and the vessel was filled with fresh propylene. The whole process was repeated every three cycles [128]. Chunan Ma et al. prepared WC using AMT (ammonium meta tungstate) and deionized water.

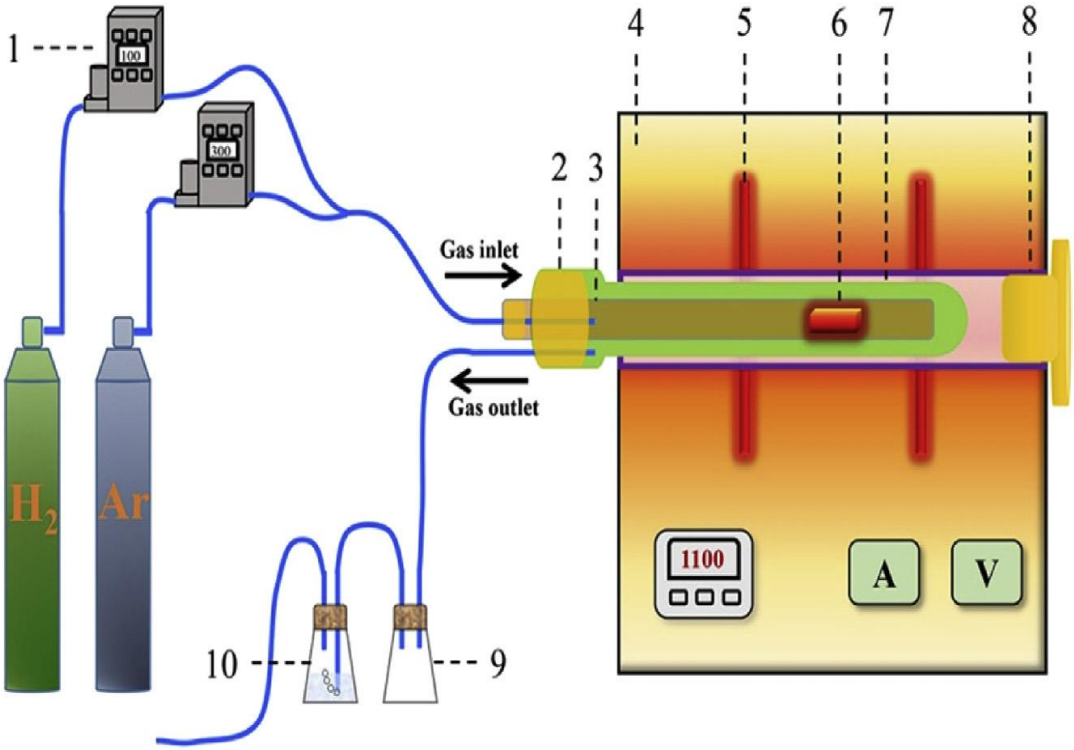

Figure 6: Synthesis of WC from WO3 and carbon black [128]

2.2.3 Chemical Vapor Deposition (CVD) Reaction Synthesis:

Generally, in the CVD process, the preparation of tungsten carbide takes place through 2 steps. First, a reducing agent, most likely Hydrogen, is used for the reduction of some type of tungsten salt and then the carburization of that tungsten salt with hydrocarbon gas. As an example, we take WCl_6 as the precursor of tungsten, so we will reduce it with the best reducing agent, i.e., H_2, and carburize it with a hydrocarbon which is methane gas. The overall reaction that will take place is as followed as

$$WCl_6(g) + H_2(g) + CH_4(g) = WC(s) + 6HCl(g)$$

If the temperature range of the above reaction is between 800 to 1200^{o}C, then the free energy of the reaction will be between -469 to -630 KJ. Basically, the supersaturated vapors formed in the vapor phase synthesis are relatively less stable than that of the solid nano powder thermodynamically. So, the molecules present in the vapor phase react and form a condensed phase. With the help of these vapor phase reactions, one can prepare nano

powder of high purity, and with these other properties can also be controlled like size, shape, reaction rate, and crystal structure.

A lot of research work has been done so far on the preparation of nano size WC using the CVD process. Usually, for the preparation of WC using CVD process materials like (WCl_6) [129], tungsten hexafluoride (WF_6) [130], or ($W(CO)_6$) [131] are generally used because they are easily reduced by hydrogen gas and have low volatilization temperature. Many other carbon source materials (hydrocarbons) like propane (C_3H_8) [132], acetylene (C_2H_2) [133], and methane (CH_4) [123, 134] are favored and used as carburizing agents. Among all these materials, methane is widely used due to its various properties in the chemical vapor deposition process [135].

Hojo et al. utilized the flow method to carry out the vapor phase reaction at a pressure of 1 atm. WCl_6 that had been reduced from the source was transported by a mixture of CH_4-Ns to the reaction zone, where it was combined with hydrogen. It was discovered that the temperatures at which the streams of WCls-CH_4-Ns + Hs were mixed influenced the qualities of the powders that were made. So the mixing was carried out using two different routes or techniques. In technique (A), the streams were mixed at a low temperature (400^oC) before entering the reaction zone. In method (B), on the other hand, the streams were combined at a high temperature in the middle of the reaction zone. The temperature of the reaction is usually the temperature present in the center of the reaction zone, ranging from 1000 to 1400^oC. By means of natural sedimentation, the powders that were created are eventually collected in a flask [129]. Won et al. synthesized WC through the vapor phase method. In the typical synthesis used by Won et al., the oxygen and water vapors were removed from the hydrogen (99.9 percent), acetylene (99.9 percent), and argon (99.9 percent) gases by passing them through copper turnings that were heated to 923 K. The temperature of the vaporizer was used to regulate the partial pressure of $WC1_6$, and the temperature of the line that connected the vaporizer and the reactor was raised to around 670^oC to prevent condensation of $WC1_6$ (B. P. = 619.9^oC). The purity of the $WC1_6$ that was utilized in this study was 99.9 percent. The reactor used in the experiment was made up of an alumina tube that had a 3 cm internal diameter and was 60 cm long. After cleaning the precursor with argon gas, the reactor was next subjected to the flow of hydrogen gas that had been saturated with $WC1_6$. A preliminary test was performed in which the start of

WC took place from WCl_6 when a mixture of C_2H_2/argon mixture was put into the reactor. This test was used to determine whether H_2 was saturated with $WC1_6$. The hydrogen chloride that was formed was absorbed in water that had been distilled, and the electrical conductivity of the solution that was produced as a result was measured to determine how far along the reaction had gotten. Because of the low temperature in the vaporizer, there was only a minute amount of hydrochloric acid created, which is shown in **Figure 07** [133].

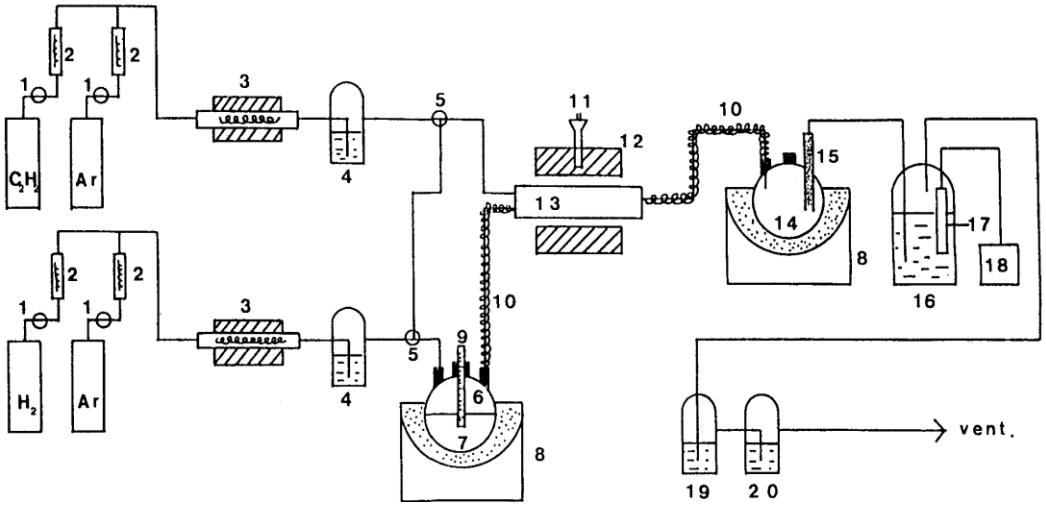

Figure 7: Schematic of the CVD Process [135]

2.2.4 Synthesis of WC Hybrids:

Zesheng Li et al. synthesized the WC hybrid using an asynchronous high-temperature technique to synthesize the WC/HMG composite support. A polystyrene (PS) microsphere was used as an atoning template during this process. Ammonium meta tungstate (AMT) and Graphene oxide (GO) were the precursors. A modified version of Hummers' process was used to create the GO, and it was then distributed in deionized water. Drop by drop, 160 mL of PS microsphere dispersion with a mean size of 3 mm and a concentration of 5 mg mL^{-1} was added to 100 mL of GO solution (2 mg mL^{-1}). Then the prepared solution was poured into a magnetic stirrer and stirred for 60 minutes. After this, 50 mg of AMT were put into the previously prepared mixed solution, and it was stirred again for 60 minutes. The prepared solution was concentrated through simultaneous heating and magnetic stirring then it was freeze-dried to remove any remaining moisture. In the end,

the product that was dried was transferred to a tube furnace, where it was heated at 850^{o}C for two hours in an argon atmosphere at a heating rate of 5^{o}C min^{-1}. To provide a point of comparability, HMG was manufactured as well by following a similar procedure as WC/HMG, but without the inclusion of AMT in the process. The WC/HMG/Pt electrocatalyst was created by using a process that involved instant microwave heating and reduction. An ultrasonic bath was used to combine a certain quantity of H_2PtCl_6 and WC/HMG with ethylene glycol for a period of 30 min. After thoroughly combining the ingredients, the solution was placed in a microwave oven, where it was heated up to the boiling point and kept at that temperature for a period of 30 sec. The product in its prepared state was washed with deionized water, followed by its drying in a vacuum. The HMG/Pt and Pt/C electrocatalysts with similar Pt content were synthesized as well so that a comparison could be made between the two. Approximately 30% of the electrocatalyst's mass was composed of platinum, according to its chemical analysis [136]. Jie Zhang et al. also prepared a hybrid of WC in nitrogen-doped carbon. The hybrid M–N–C was made by impregnating and pyrolyzing a mixture of melamine, ammonium meta tungstate (AMT), and an organic carbon source. The combination contained Fe $(NO_3)_3.9H_2O$, $Co(NO_3)_2.6H_2O$, and $Fe(NO_3)_3.9H_2O$. The carbon source for the polycondensation polymerization process was resorcinol–formaldehyde resin and silica was employed as the rigid template for the material. In the beginning, distilled water was used to dissolve 500 mg (3.96 mmol) of melamine, 0.835 g of AMT, as well as a specific amount of silica and Fe $(NO_3)_3.9H_2O$/Co $(NO_3)_2.6H_2O$. After that, 0.550 gm of resorcinol and 0.95 mm of formaldehyde diluted to 37% in water were mixed into the aqueous solution while it was being stirred. After the reaction was completed, the fluid was poured into a beaker and heated to 85^{o}C for 3hr. Following the termination of the reaction, the solution mixture was heated to 80^{o}C for an entire night in order to eliminate the solvent, and then it was calcined at temperatures ranging from 700 to 900^{o}C for 3 hrs. The silica particles were removed from the synthesized composites by first washing them in 30 mm of 1M (KOH) at a temperature of 120^{o}C for 3 hrs. After that, the composites were washed in distilled water until the pH of the solution became neutral. After drying in a vacuum oven for one night, the product was then named Fe/Co/WC@NC [137]. Feng long Sun et al. synthesized a hybrid of WC and cobalt that was saturated with carbon. In this study, the following steps

were taken to get the mixture: The raw material, i.e., WC powder, was mixed well with graphite and Co (the mass ratio of graphite, WC, and Co, is 0.1:1:1), and the powder was then crushed for 30 minutes with a ball crusher. The number of charges to balls stayed at 20:1. 150 g of the above graphite/WC/Co powder was packed into a corundum crucible and heated in a furnace at a temperature of 1700°C for 2 hours in the reduction media. Then it was cooled down at a rate of 2°C/min. When the temperature of the metal was reduced to room temperature, deionized water was used to wash it. For metallographic study, a piece of the C/W/Co alloy was cut and polished. The alloy was electrolyzed in order to get WC powder. The electrolyte used in this electrolysis process was $CoCl_2$, an alloy of WC that was acting as an anode, and titanium acted as a cathode, and the time of the completion of the whole process was 120 hrs. The powder that didn't dissolve was first washed and then dried. In the end, the dried powder was treated with 98 percent sulfuric acid (H_2SO_4) at 250°C by dropping nitric acid (HNO_3) for the removal of free graphite [138]. Can Liu et al. synthesized WC carbon composite for hydrogen evolution reaction (HER). Chemical oxidative polymerization was the most common way for the production of polyaniline from aniline. In the meantime, the sulfuric acid that was prepared reacted with the soluble sodium tungstate to make hybrid precipitates that were made up of insoluble PANI and undetectable H_2WO_4 [139]. Young-Jin Ko et al. also synthesized a WC hybrid with nanowall. In the typical preparation, Tungsten carbide nanowall film was made on an NCD-coated Si wafer using a surface-carburized tungsten cathode and direct current plasma-assisted CVD (DC-PACVD). This is how WC nanowalls are usually made. In the CVD chamber, the substrate was exposed to the hydrogen plasma. The total amount of hydrogen gas moving through the chamber was 150 SCCM, and the pressure in the chamber was 100 Torr. The details of the whole process that how it is prepared, what is essential for the growth of the catalyst, and all the characterizations are reported [140]. Peng Xiao et al. prepared WC–MOC composite. It is usually made by mixing $(NH_4)_6Mo_7O_{24}.4H_2O$ and $Na_2WO_4.2H_2O$ together. This makes nanowires of molybdenum-tungsten complex oxides while using $(NH_4)_6Mo_7O_{24}.4H_2O$ alone only makes a much larger micro belt of MoO_3. It was seen that the shape of the precursor did not change by varying its molar ratio. For our ease, the samples are named by the molar ratio of tungsten to molybdenum that is present in the precursor. The nanowires of molybdenum-tungsten

complex oxides with a molar ratio of 1:2 and 1:4 (W: Mo) are called nw-W_2MoO_3 and nw-W_4MoO_3, while their corresponding carbides are called nw-W_2MoC and nw-W_4MoC. The nw-W_4MoC and nw-W_2MoC keep their structure of interwoven nanowires with the mean size of 15–20 nm after they are carburized. **Figure 8** shows the preparation procedure used by Peng Xiao [141]. Abdullah M. Al-Enizi et al. prepared graphene and WC composite. In its typical synthesis method, graphene and WC were suspended in 100 mL of 5 M KOH solution to make 5, 10, and 20% graphene/WC. They were named as 5%, 10%, and 20% WC@GNFs. After 1 hour of stirring, the slurries were sonicated again for 1 hour. The produced slurries were then heated in a microwave oven in a single continuous pulse for 50 s. The produced slurries were subsequently heated in a muffle furnace (Carbolated, Thermo Fisher Scientific, 1400^oC, USA) for 24 hours at 120^oC. Then they were allowed to cool naturally, filtered, and washed with distilled water. The prepared nanocomposites were then dried at 50^oC overnight under vacuum [142].

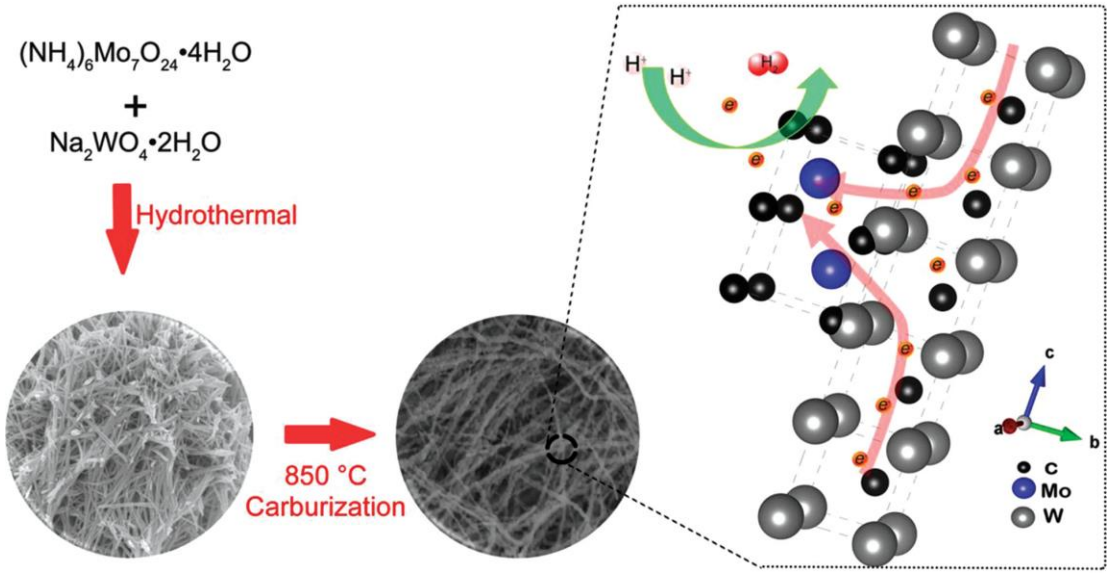

Figure 8: Synthesis of WC and molybdenum carbide composite [143].

2.3 Electrochemical Activity

Tao Zhao et al. prepared WC hybrids using two different temperatures and compared the electrocatalytic activity of both the samples. In his paper, he reported that the WC hybrid prepared at 800^oC has low Tafel slope of 75.5 mV/dec than the one prepared at 600^oC (96.2

mV/dec). He also added that the overpotential also followed the same trend as that of the Tafel slope. The overpotential of the WC (800) was 375 mV, and that of the WC (600) was 495 mV for an OER reaction **Figure 9** shows the results illustrated by Tao Zhao et al.[143]. Soumyabrata Roy et al. reported the activity of HER and OER of Ni substitute in tungsten carbide in an alkaline solution. In his paper, he reported a lower Tafel slope of 135 mV/dec for Ni-WC and an onset potential of 120 mV for HER and a Tafel slope of 57 mV/dec and an overpotential of 310 mV for OER. The overall results are shown in **Figure 10** [144].

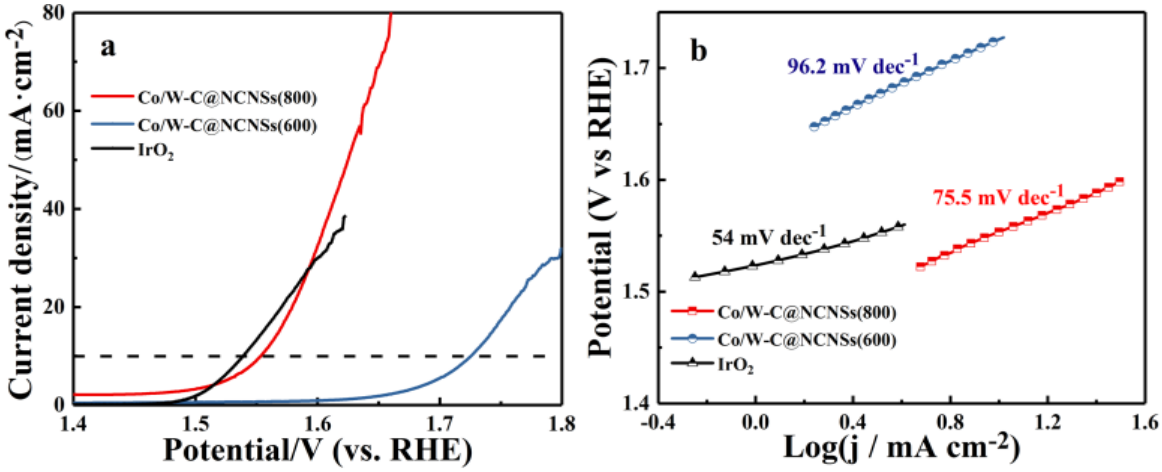

Figure 9:Polarization curves of the prepared samples for OER (b) Tafel slope of the corresponding samples for OER [145].

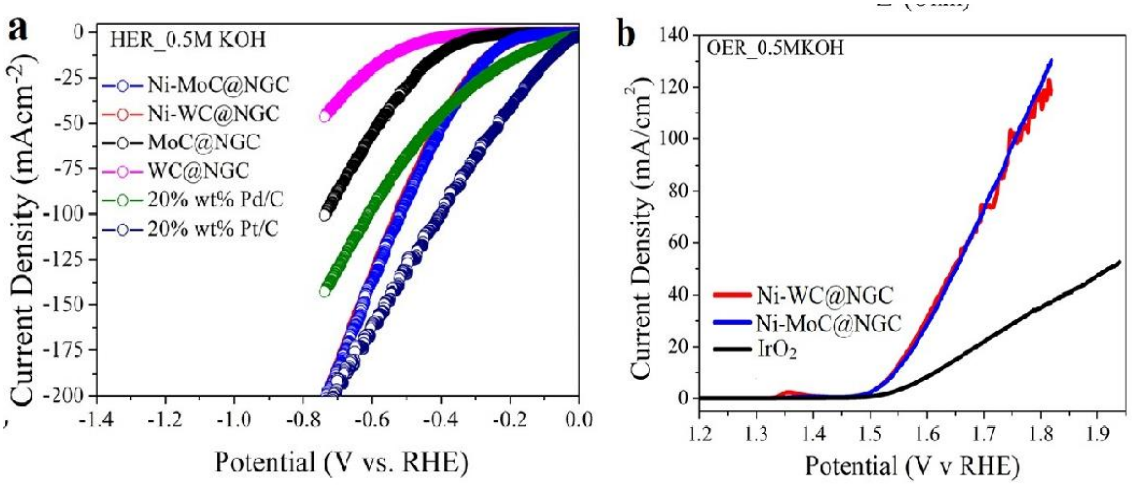

Figure 10:(a) Polarization curves of different materials for HER. (b) corresponding polarization curves for OER [146].

Jin Soo Kang et al. prepared nanoporous tungsten carbide. They reported that the overpotential of WC was 187.1 mA cm^{-2}/ mV and its Tafel slope was 87.8 mV/dec [145]. Lulu Qiao et al. reported that the OER overpotential of nanohybrid WC was 238 mV and its Tafel slope was 59 mV/dec. The same sample gave an overpotential of 98 mV at a current density of 10 mA/cm^2 and a lowest Tafel slope of 50 mV/dec for an HER reaction. **Figure 11** shows the polarization curves and Tafel slopes of OER and HER, respectively [146]. The overpotential of tungsten carbide reported by lee et al. was 444 mV with a current density of 20 mA cm^{-2} in 0.1 M H_2SO_4 electrolyte [147]. A composite of MoS_2/WC/RGO prepared by Yan et al. in his research showed that the composite had excellent HER activity with a Tafel slope of 41 mV/ dec in 0.5 M H_2SO_4 and an onset potential of -0.11 V [115]. Jiabo Wang et al. also showed that making a composite of WC gives good HER and OER activities. In his research, he made a composite of N doped graphene with W_xC, which showed the smallest overpotential of 77 mV at a current density of 10 mA/cm^2 for HER, and the Tafel slope of this composite was observed to be 45.91 mV/dec, which was the smallest in all the samples prepared. Similarly, for OER, an overpotential of 467.6 mV was observed for the current density of 10 mA/$cm^{2,}$ and the Tafel slope of the sample, in this case, was 36.2 mV/dec [148]. A hybrid named W_2C/MWCT was prepared by Qiu fang Gong, the Tafel slope of which was determined to be 45 mV/dec, and the overpotential of the prepared hybrid was reported to be 123 mV at a current density of 10 mA cm^{-2} in 0.5 m H_2SO_4 electrolyte [149, 150]. Yan-Tong Xu prepared WC@NPC and performed its electrochemical analysis. He observed that the prepared sample had good HER performance with an overpotential of 51 mV at a current density of 10 mA cm^{-2}, which was the smallest in all the prepared samples, and the Tafel slope of this sample was examined to be 49 mV/dec [106]. Meng qi Zeng et al. produced a second hybrid of tungsten carbide and graphene, WC/graphene, and examined its Tafel slope and overpotential. According to him, a low overpotential of 120 mV and a Tafel slope of 38 mV/dec indicated that the sample has exceptional catalytic characteristics [113]. P. Bretzler produced tungsten carbide and conducted the CsH_2PO_4 electrochemical investigation. He showed that in the given electrolyte, WC possessed good activity because of tungsten carbide in CsH_2PO_4. Further, he observed that the electrochemical study was strongly dependent on temperature. The cyclic voltammetry of the prepared catalyst is

shown in **Figure 12** [151]. **Tables 3** show the electrochemical performances of some WC catalysts and their hybrids for both HER and OER reactions.

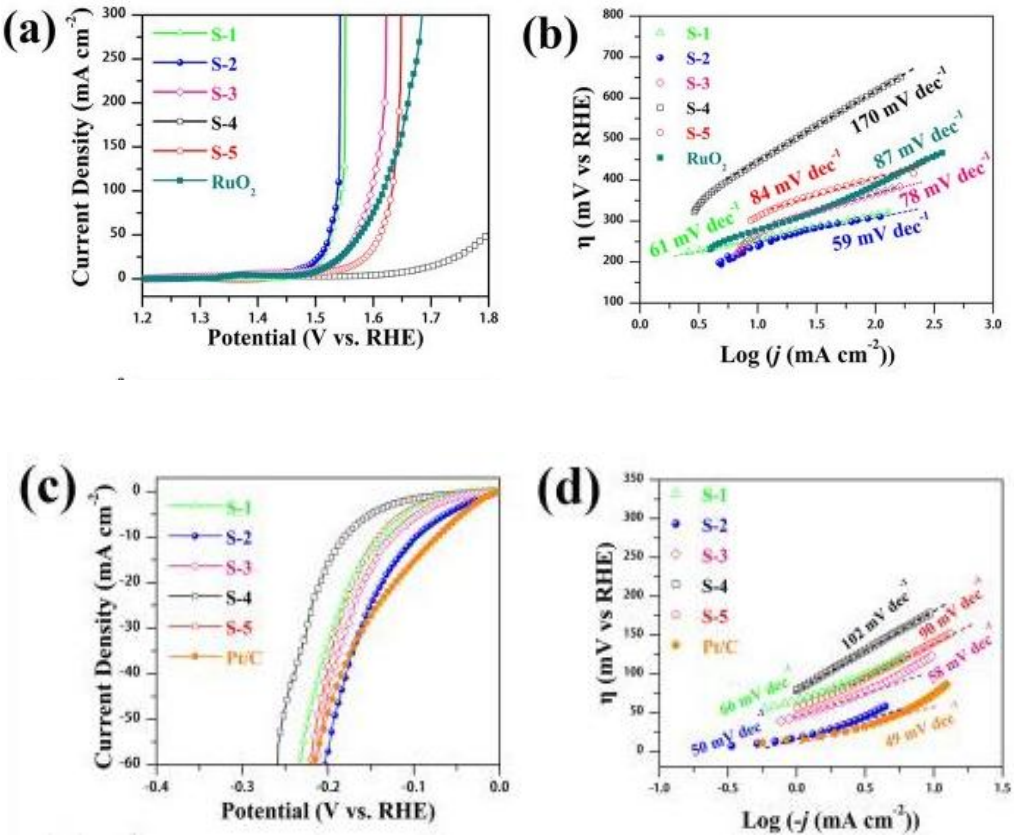

Figure 11: a) LSV polarization curves of OER, (b) the corresponding Tafel plots for OER, (c) LSV polarization curves (d) the corresponding Tafel plots [148].

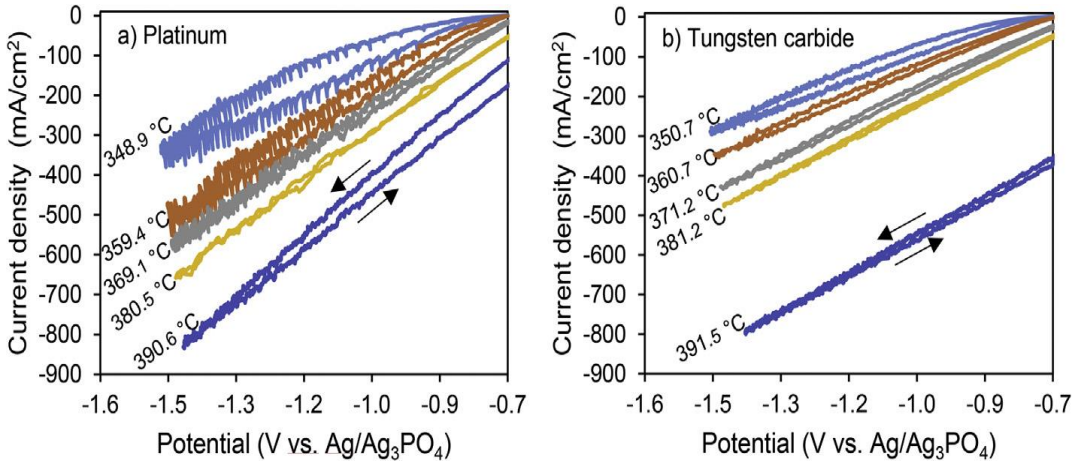

Figure 12:Cyclic voltammetry curves for (a) platinum and (b) tungsten carbide cathodes in molten CsH2PO4 at increasing temperatures [152].

Table 3: Electrochemical Water Splitting Performance of WC and its Hybrid for HER and OER.

S.no	Catalysts	Target reaction	Over potential (mV)	Tafel slope (mV/dec)	Current density mA/cm^2	Electrolyte	Ref
1	W_xC/NG	HER	77.82	45.95	10	0.5 M H_2SO_4	[148]
2	N-WC nano array	HER	89	75	10	0.5 M H_2SO_4	[152]
3	P-W_2C	HER	55	39	10	0.5 M H_2SO_4	[153]
4	WC-W_2C/PNCDs	HER	101	90	10	1 M KOH	[154]
5	W_2N/WC	HER	148.5	47.4	10	1 M KOH	[155]
6	ES-WC/W_2C	HER	75	59	20	0.1 M KOH	[156]
7	WC_x/C	HER	264	85	10	0.5 M H_2SO_4	[157]
8	WC nanowalls	HER	160	67	10	0.5 M H_2SO_4	[140]
9	WC microsphere	HER	50	118	1	1 M H_2SO_4	[158]
10	WC commercial	HER	100	73	1	1 M H_2SO_4	[158]
11	WC-CNT	HER	489	122	10	0.5 M H_2SO_4	[159]
12	CNS@WC/GF	HER	65	61	10	1 M H_2SO_4	[160]
13	WCh_s	HER	80	89	1	0.5 M H_2SO_4	[161]
14	WC nanocrystalline	HER	248	-	10	0.5 M H_2SO_4	[140]
15	7.5 wt% Pt/W_2C	HER	5	103	1	1 M H_2SO_4	[158]
16	Pt/WCh_s	HER	22	27.1	20	0.5 M H_2SO_4	[161]
17	Fe-WCN	HER	100	47	10	1 M H_2SO_4	[162]
18	WC/CB	HER	175	-	1	0.5 M H_2SO_4	[163]
19	WC	HER	100-150	84	38.5	0.5 M H_2SO_4	[127]
20	N-WC nanoarray	OER	470	-	60	0.5 M H_2SO_4	[152]
21	W_2N/WC	OER	320	94	10	1 M KOH	[155]
22	Co/W-C@NCNSs	OER	323	75.5	-	1M KOH	[164]

Chapter 3

Material and Methodology

3.1 Materials:

The chemical and reagents used in this research are Ammonium meta tungstate dihydrate (AMT) purchased from sigma Aldrich, Fructose, Potassium hexacyanoferrate tri hydrate (PHCF) ($K_4[Fe(CN_6).3H_2O]$), terephthalic acid (BDC) ($C_8H_6O_4$) from Merck, Zirconium chloride $ZrCl_2$, Dimethylformamide (DMF)(C_3H_7NO) from Merck, Acetic acid (CH_3COOH), Ethanol (C_2H_5OH) from BDH, Hydrochloric acid (HCL), Polyvinylidene fluoride (PVDF)$(C_2H_2F_2)n$ from sima Aldrich, N-methyl-2-pyrolidone (NMP)(C_5H_9NO) from Merck, Activated carbon from Duksan pure chemicals, and deionized water from Sigma Aldrich.

3.2 Synthesis of pure Tungsten Carbide (WC):

For the synthesis of pure tungsten carbide precursor was synthesized first using hydrothermal method then calcinate this precursor using solid gas reaction. Precursor is prepared by mixing 5 g AMT and 4.6 g fructose in deionized water. After proper mixing poured the solution to a Teflon lined autoclave and heat it for 12 h at 220^oC. after the completion of the reaction the prepared precursor was washed with ethanol and deionized water 3 times each and then dried at 70^oC overnight. Now put this precursor in a tube furnace and heat it at 1050^oC for 2 h under Ar/H_2 environment. The flow rate of Ar/H_2 is 3/1 throughout the reaction. Over all schematics is given in **Figure 13**.

3.3 Synthesis of Pure Prussian Blue (PBNPs):

In the preparation of pure Prussian blue 2 mmol of potassium hexacyanoferrate trihydrate is dissolved in 100 ml HCl (0.1) solution. The solution is then sonicated for 8 h in ultra-sonication bath. After the completion of sonication, the blue colour product is washed with ethanol and deionized water and dried in vacuum oven at 40^oC overnight.

3.4 Synthesis of Pure UiO-66:

This MOF was synthesized using solvothermal method. In this method 150 mg Zirconium chloride (ZrCl4) and 115 mg of terephthalic acid (BDC) was dissolved in 30 ml of DMF solvent. Add 2 ml Acetic acid to the above solution and mix it for 2 h followed by 20 minutes ultra-sonication. After 20 minutes sonication transfers the solution to 100 ml of Teflon lined autoclave and heat it at 120^{o}C for 24 h. after the completion of the reaction washed the prepared product with DMF and ethanol to remove extra ions and any non-reacted reactants and then dried at 70^{o}C overnight in oven.

3.5 Synthesis of WC and Prussian blue Hybrids:

Hybrids are prepared through in situ technique in which we grow WC on Prussian blue cubes. Three hybrids are synthesized containing different ratios of WC and potassium hexacyanoferrate trihydrate. Hybrid with equal ratio of WC and PHCF (1:1) is named as WC 1, hybrid with ratio of WC to PHCF (2:1) is named as WC 2, and hybrid with ratio of WC to PHCF (1:2) is named as WC 3. All the hybrids are prepared using same procedure with varying quantities of WC and PHCF. In the typical synthesis of hybrid WC 1 dissolve 2mmol of WC in 100 ml HCL solvent(0.1molar) and then add 2 mmol PHCF in it and sonicate it for 8 h in ultra-sonication bath. After 8 h washed the solution with deionized water and ethanol and then dried it at 40^{o}C overnight. In WC 2 4 mmol of WC is used and in WC 3 4 mmol of PHCF is used the rest of the procedure is same as that of the WC1.

3.6 Synthesis of WC and UIO-66 Hybrids:

Hybrids of WC with UiO-66 are also synthesized using hydrothermal method. WC 4 is the hybrid with WC/$ZrCl_4$ equal to (1:1), WC5 have ratio of WC/$ZrCl_4$ equal to (2:1), and WC6 have WC/UiO-66 ratio equal to (1:2). In the typical synthesis of WC 4 equal amount of WC and $ZrCl_4$ is taken and mixed in 30 ml DMF already contain 115gm BDC. Then add 2 ml Acetic acid to the solution and mix it for 2 h. After proper mixing sonicate the solution for 20 minutes. Now the solution was transferred to Teflon lined stainless steel autoclave and heat it for 24 hours at 120^{o}C. When the reaction is completed cool the autoclave to room temperature and wash the solution with DMF and ethanol several times. After complete washing dry the product at 70^{o}C for 24 h in oven. In WC 5 the amount of

WC is double to that of $ZrCl_4$ and in WC 6 the amount of $ZrCl_4$ is double to that of the WC and the rest of the procedure is the same as that of WC 4.

3.7 Preparation of electrode:

In the preparation of working electrode first ink was prepared and then it was deposited on treated Nickle foam. Nickle foam was treated before the deposition with HCL and ethanol. In the ink preparation 2.5 mg of PVDF, 5 mg of carbon black and 42.5 mg of prepared catalyst were mixed in 0.3 to 0.4 ml of NMP solvent and sonicate it for 4 h in ultra-sonication bath. After 4 h the prepared ink was deposited on Nickle foam. After the deposition the catalyst was dried at 80^{o}C overnight and press under 1 bar pressure before use.

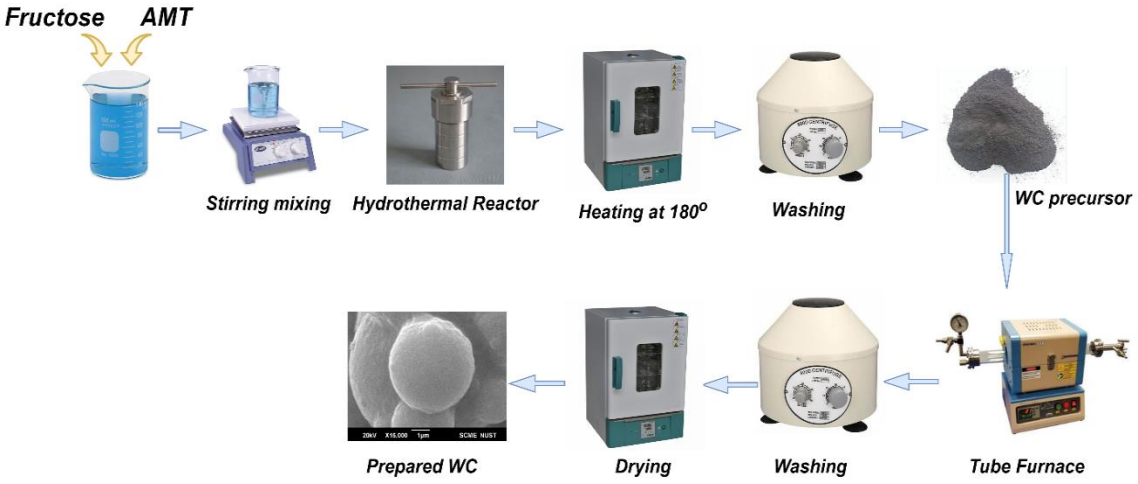

Figure 13: Process Flow of the Method Used for the Preparation of Catalyst.

Chapter 4

Result and Discussion

4.1 Material Characterization:

For the detailed study of material nature X-ray diffraction (XRD) (STOE-SEIFERTX PER PRO) is used. This XRD is used for the compositional analysis, Phase formation and for the crystallinity of the prepared catalyst. Cu-Kα radiation is employed in the process with 2θ values in the range on 0 to 90^{o}. for the morphological study and elemental analysis of the prepared catalysts scanning electron microscopy (SEM) (JEOL-JSM-6490A) was used coupled with Energy Dispersive X-ray (EDX).

4.2 Electrochemical Analysis:

For the electrochemical study of the fabricated catalysts Origa lys (model number 5) is used with three electrode assembly. The working, counter electrode and reference electrode. Catalyst that was deposited on the Nickle foam is used working electrode in the process. The reference electrode is Ag/AgCl and platinum wire is used as a counter electrode. We use 1 molar KOH solution as electrolyte in our experimentation process. The potential was converted to a reversible hydrogen electrode (RHE) for easy computations. The equation for RHE used is as follows

$$ERHE = E_{Ag/AgCl} + 0.059*PH + E^{o}_{Ag/AgCl}$$

In the given equation PH is 14 and the value of $E^{o}_{Ag/AgCl}$ is 0.1976.

Tests that are performed for the electrochemical characterization of the fabricated catalysts are linear sweep voltametery (LSV), Cyclic Voltametery (CV), Chronopotentiometry, and electrochemical impedance spectroscopy (EIS). LSV was performed at 10 mV/s scan rate with a potential range of 0 to 1.5 V. CV was performed at different scan rates with a potential range of 0 to 0.6 V. Tafel slope was calculated using equation: $\eta = c \log I + a$

Here η is the over potential, I is the current, a is Tafel constant, and c is the Tafel slope.

Over potential is plotted on Y-axis and log of current density on X-axis.

EIS was performed at a voltage amplitude of 10 V and a frequency range of 0.1 Hz to 2 M Hz. For checking the stability of catalyst chronopotentiometry was performed for 24 h.

4.3 Results and Discussions:

4.3.1 Phase Determination and Crystal Size:

X-ray diffraction technique was used to determine the Phase and the crystal structure and crystal size of the prepared catalyst. **Figure 14 (a)** shows the XRD pattern of pure tungsten carbide powder. These peaks are in correspondence with hexagonal crystal plane of WC (JCPDS 65-4539). The peaks appeared at 2θ angles of (31.3), (35.7), (48.2), (64.1), (65.4), (73.1), (75.6), (84.1) corresponding to the planes of (001), (100), (101), (110), (111), (200), (102), (201) respectively. The occurrences of these peaks at the given planes and angles conform the fabrication of hexagonal WC confirmed from literature [165]. **Figure 14 (b)** shows the XRD pattern of prepared pure Prussian Blue. This figure shows that peaks appeared on the planes (200), (220), (400), (420), (422), (440) and (600) corresponding to the angle of 2θ values of (24.8), (26.5), (28.1), (36.6), (43.6), (47.8), and (51.8) respectively. these peaks are in correspondence with JCPS card number (73-0687) which conform the synthesis of pure Prussian blue (PBNPS) also confirmed form literature [166]. The XRD pattern of pure UiO-66 is shown in **figure 14 (c).** the figure shows that planes (111), (002), (006), and (110) were indexed at 2θ values of 7.4º, 8.4º, 26º, and 44.2º. The values were in corresponding with the values of literature which confirm the formation of UiO-66. **Figure 14 (d), (e), (f), (g), (h), (i)** shows the XRD pattern of the prepared hybrids i.e., WC 1, WC 2, WC 3, WC 4, WC 5, and WC 6. In all the hybrids of WC with PBNPs the peaks are appeared at 2θ angle of (24.8), (31.5), (35.6), (48.2), (64.1), (65.4), (73.1), (75.6), (84.1) corresponding to the planes of (200), (001), (100), (101), (110), (111), (200), (102), (201) respectively. The presence of 200 plane at 2θ angle of 24.8 is the prominent peak of PBNPs in all the samples while the peaks at 35.6, 48.2, and 64.1 are the prominent peaks of WC which conform the synthesis of our hybrid. Moreover, from these peaks we can also conclude that no change in the crystal structure appear in WC after the modification of PBNPs. The slight shift in the prominent peak of WC near 35º in all the hybrids compared to the pure is due to the increased crystal size. Compared to the hybrids of PBNPs there is a large shift in all the peaks of UiO-66 hybrids i.e., WC 4 and WC 6

toward the right. And this shift indicate the decrease in the crystal structure and results in larger surface area which enhance the catalytic activity. Here in WC 4 and WC 6 the prominent peaks were appeared at 2θ values of 34^{o}, 37.1^{o}, 53.1^{o}, and 73.2^{o} corresponding to the planes of 001, 100, 101, and 110 respectively. while in Hybrid WC 5 shift can be seen only in the peak appear at 35o this is because WC is present in higher ratio in this hybrid, so no shift occurs in other peaks and is the same as that of pure WC peaks. The average crystallite size of all the samples was calculated using X-ray broadening technique through Scherrer's equation [167].

$L = (K.\lambda)\ (FWHM)(\cos\theta_B)$

In this equation L is the crystallite size

K is the Scherrer's constant, and its value is 0.9 (shape Factor)

λ is the wavelength of X-rays and its value is 0.15406(nm).

FWHM is the full width at half maxima.

θ_B is the Bragg angle.

The calculated average crystal size of pure WC, pure PBNPs, WC 1, WC 2, WC 3, WC 4, WC 5, and WC 6 are (617), (387), (533.85), (704.428), (552), (249.166), (371.8), and (246.833) respectively detailed is given in **table 4**.

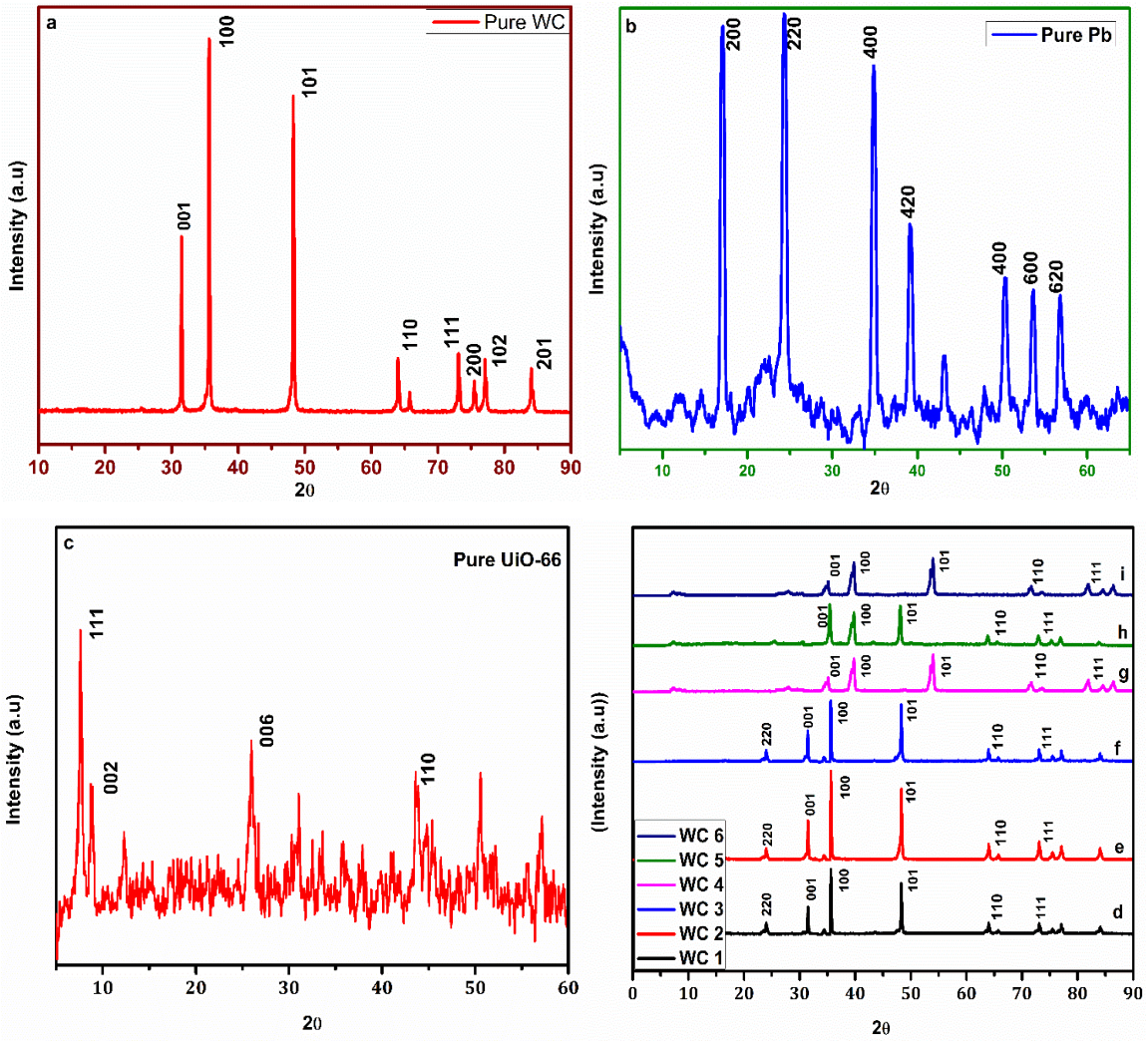

Figure 14:XRD of the (a) Pure WC, (b) Pure PBNPs, (c) Pure UiO-66, (d) Hybrids.

Table 4: crystal Size and peak position and FWHM of the prepared samples.

Electro catalyst	Peak Position	FWHM	Crystal Size	Average Crystallite Size Aº
Pure WC	31.492, 35.634, 48.264, 63.993, 73.068	0.146, 0.182, 0.182, 0.109, 0.178.	598, 480, 500, 927, 582.	617.4

Pure PBNPs	17.5,24.35, 34.8,39.22,50.33,53.9	0.14,0.189,0.189,0.189,0.582,0.287	574,430,411,446,151,310	387.0
WC 1	31.492, 35.643, 48.264, 63.993, 73.068, 30.663, 34.826.	0.182, 0.182, 0.255, 0.109, 0.146, 0.218, 0.218.	474, 480, 352, 927, 716, 392, 396.	533.85
WC 2	31.513, 35.434, 48.264, 64.011, 73.068, 65.833, 84.055.	0.146, 0.146, 0.146, 0.109, 0.109, 0.291, 0.133.	598, 605, 631, 928, 979, 334, 856.	704.428
WC 3	31.486, 35.634, 48.264, 63.976, 73.068, 30.976, 43.376.	0.146, 0.146, 0.218, 0.146, 0.109, 0.218, 0.437.	598, 605, 415, 679, 979, 393, 199.	552
WC 4	7.34, 25.32, 31.24, 35.40, 48.08, 72.934.	0.437, 0.583, 0.291, 0.291, 0.328, 0.328.	186, 142, 291, 295, 272, 309.	249.166
WC 5	7.35, 25.32, 31.245, 35.407, 48.08, 72.934.	0.437, 0.583, 0.157, 0.22, 0.22, 0.189.	186, 142, 554, 393, 410, 546.	371.8
WC 6	7.5, 25.22, 31.24, 35.40, 48.08, 72.934.	0.537, 0.553, 0.241, 0.251, 0.318, 0.318.	182, 138, 291, 295, 265, 310.	246.833

4.3.2 Morphological Study and Energy Dispersive X-ray (EDX):

Scanning electron microscopy was used to study the morphology of the fabricated samples. **Figure 15 (a)** shows the SEM image of pure WC. From the figure it is clear that the prepared WC has spherical shape cubes of non-uniform sizes. The figure also tells us that powder of WC combines to form cluster of WC particles. **Figure 15 (b)** is the SEM image of pure UiO-66. Spheres of UIO-66 can be clearly seen same is reported in the literature. **Figure 15 (c)** is the SEM image of Pure PBNPs. From the figure cubes of PBNPs with unform size can be seen clearly such cubes are also reported in literature [168, 169]. **Figure 15 (d), (e), (f)** are the SEM images of hybrids WC 1, WC 2, and WC 3. In all the images

both the compounds mixed with each other and form shapeless particles. The improper shapes are due to the synthesis route for the preparation of hybrids. In WC1 and WC2 none of the compound is dominant on the other while in WC 3 cubes of PBNPs can be seen with WC particles fused on the surface of cubes. Due to these cubes like structure formation surface area of this hybrid is increased and, in the result, it gives better activity compared to WC 1 and WC 2. **Figure 15 (g), (h), (i)** are the SEM images of WC 4, WC 5 and WC 6. As in the WC 5 the percentage of WC is greater as compared to that of UiO-66 so we can clearly see that the WC particle completely suppress the particles of UiO-66 and as a result sphere cannot be clearly seen as can be seen in WC 4 and WC 6. In case of these hybrids small clusters are formed compared to the hybrids of PBNPs and because of that it provide greater surface area than the hybrids of PBNPs

Energy Dispersive X-ray (EDX) of the best catalyst i.e., WC 3 is performed to confirm that our hybrid has all the necessary elements. The result of EDX shows that hybrid WC 3 is composed of tungsten (W), Carbon (C), and iron (Fe). The atomic percent of W, C and Fe is 40.3, 2.6 and 57% as shown in **figure 15 (k).** This shows that the all the three components are present in the sample which confirmed the successful synthesis of WC and PBNPs hybrid. The weight percentage of W, C, and Fe in the sample was 89, 8, and 2 percent. As iron and tungsten both are very good conductor so due to their synergistic effects the charge transfer ability of the is enhanced in the result electrocatalytic performance is improved even further. **Figure 15 (j)** is the EDX of WC 4 in which the percentage WC and Zr is given. The result tell us that the hybrid is composed of W, C, Zr, and O with atomic weight percent of (9.8), (67.9), (4.4) and (17.9) respectively. and the weight percentage of all these elements are (54.5), (24.7), (12.1), and (8.7).

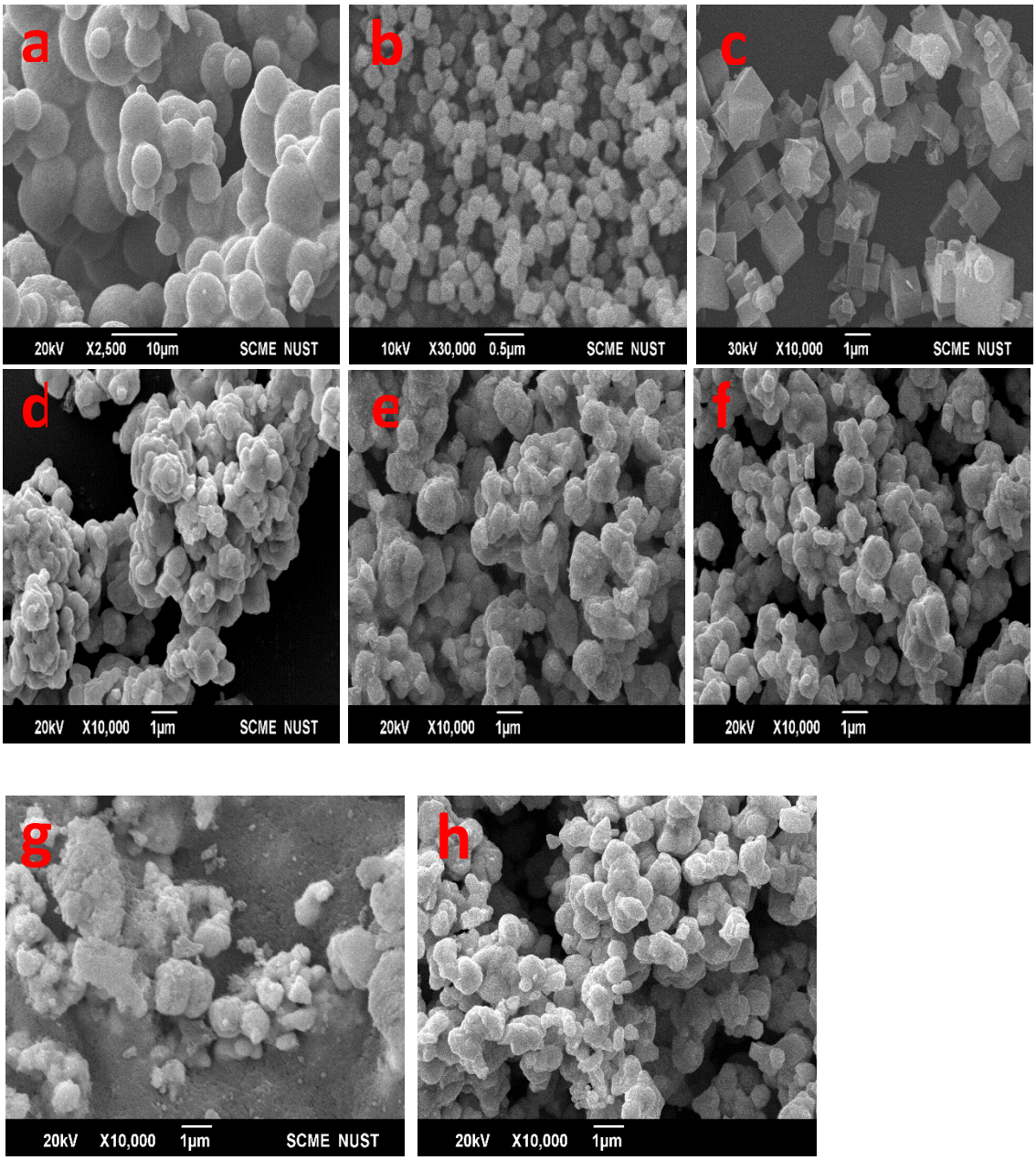
a
20kV X2,500 10μm SCME NUST
b
10kV X30,000 0.5μm SCME NUST
c
30kV X10,000 1μm SCME NUST
d
20kV X10,000 1μm SCME NUST
e
20kV X10,000 1μm
f
20kV X10,000 1μm
g
20kV X10,000 1μm SCME NUST
h
20kV X10,000 1μm

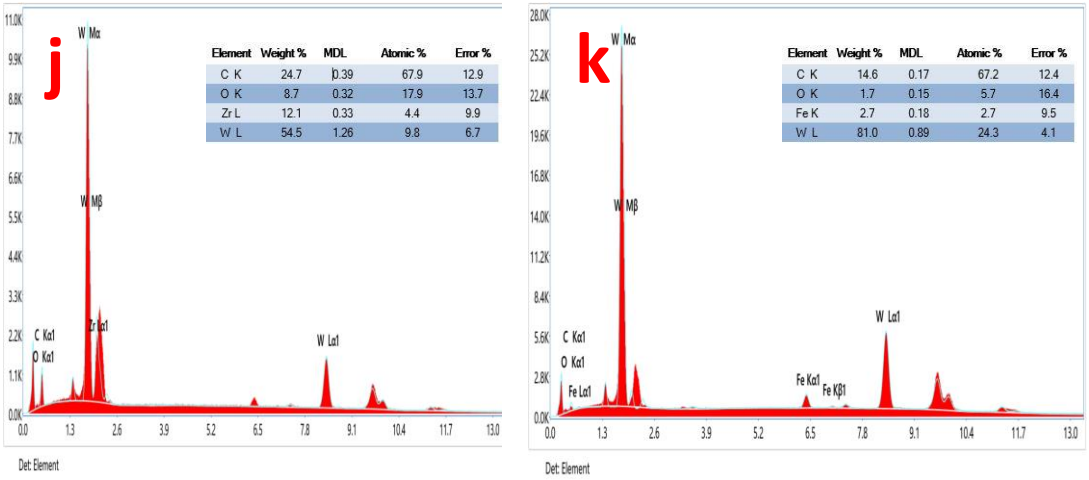

Figure 15: (a-i) SEM images of all the prepared hybrids and pure samples (J, k) EDX of WC 4 and WC 3.

4.4 Electrochemical Study:

4.4.1 Hydrogen Evolution Reaction:

For the electrochemical study of pure WC, pure PBNPs, Pure UiO-66 and their hybrids a three-electrode assembly is used in 1 molar KOH solution. **Figure 16 (a, b)** shows linear sweep voltametery curves of HER. From the figure it is clear that the prepared hybrids have greater activity as compared to pure WC, pure PBNPs, and pure UiO-66. The overpotential reported of pure WC, pure PBNPs, and pure UiO-66 is 24, 209 mV, and 201mV at 10 mA/cm^2 current density. The hybrids WC 1, WC 2, WC 3, WC 4, WC 5, and WC 6 have over potential of 207, 178, 162, 144, 161, and 104 respectively at a current density of 10 mV/cm^2. Compare to other hybrids WC 6 possess least over potential of 104 mV representing good HER activity. Tungsten carbide is one of the best conducting materials that's why electron charge transfer occur easily and give us low over potential. Moreover, WC, Zr and Fe all materials are the active site for hydrogen evolution reaction. In the structure of PBNPs there are two oxidation states of iron i.e., (Fe^{2+} and Fe^{3+}). With carbon the oxidation state of iron is +2 and with nitrogen +3 oxidation state of iron is present. The oxidation state of W is +4 with carbon in WC. The oxidation of Zr is also +4 with oxygen in UiO-66. Due to greater number of active sites in Prussian blue and UiO-66 compared to WC the electron transfer due to these compounds is faster as compared to electron transfer in WC as a result higher reduction of H^+ to H_2 occur in them. Therefore,

the HER activity of PBNPs and UiO-66 is higher than that of WC as can be seen in the figure 3. The increased electro catalytic hydrogen generation is ascribed to the increased number of active sites in nanocomposites (WC@UiO-66) and compact heterojunctions between WC and UiO-66. This increase could be attributable to more active edge sites on the surface of the UiO-66 and WC which limit charge carrier recombination and quick charge carrier migration, resulting in better electro catalytic H_2 generation. Further the activity of the hybrids of UiO-66 is grater than that of the hybrids of PBNPs because of the larger surface area of Zr MOF and its porous nature as compared to Fe MOF. So the exposed active sites are more in the UiO-66 which results in rapid electron transfer and give us a low over potential of 104 mV.

To further study the catalytic activity of the prepared hybrids Tafel slope is calculated using the following equation [169]

$\eta = c \log I + a$

here is the over potential, c is the Tafel slope, I is the current density and a is the Tafel constant.

In general, Tafel slope is inversely proportional to the activity of a catalyst. The lower the Tafel slope of a catalyst the higher the activity of that catalyst. Tafel slope corelates over potential with reaction rate. The mechanism of HER reaction can be found out using Tafel slope because it also tells about the rate limiting step of HER. Smaller Tafel slope mean high electron transport mean high activity of the catalyst with low over potential. The Tafel slope of the prepared catalyst for HER is shown in **figure (e, f)**. Form the figure it is clear that pure WC have the highest Tafel slope and hybrid WC 6 has the lowest Tafel slope among all the fabricated catalysts i.e., 43 mV/dec. Tafel slope of pure WC, Pure PBNPs, pure UiO-66, WC 1, WC 2, WC 3, WC 4 and WC 5 are (116), (106), (109), (79), (71), (67), (62) and 85 mV/dec respectively. these values of Tafel slope confirmed that hybrid WC 6 gives the highest activity and pure WC shows least activity among the prepared set of catalysts. Because of the low slope of WC 6 i.e., 43 mV/dec it follows Volmer-Heyrovsky mechanism [170]. The over all kinetics of the reactions are given as

Volmer Step: $H_2O + M + e^- \rightarrow M\text{-}H + OH^{-1}$

Heyrovsky Step:

$H_2O + M + -H_{ads} + e^- \rightarrow H_2 + OH^{-1}$.

In the above equations M is our working electrode which work as adsorption sites for water molecules. The water molecule in the KOH solution dissociates on the surface of working electrode into adsorbed hydrogen and hydroxyl free ion in the Volmer step, and then that adsorbed hydrogen interacts with more molecules of water and reduced to hydrogen molecule and another hydroxyl ion in the Heyrovsky step. From the literature it was studied that the dissociation of water in the Volmer step can be enhanced by using WC and its hybrids with various MOFs. This is because of the conductive nature of WC and large surface area and porous nature of MOFs. Supporting this literature study our prepared hybrids of WC with PBNPs i.e., WC 3 and with UiO-66 i.e., WC 6 both shows outstanding results due to the synergistic effects of both materials in both the hybrids.

4.4.2 Oxygen Evolution Reaction:

The performance of OER of the prepared hybrids is also find out using linear sweep voltametery in 1 molar KOH (alkaline) electrolyte. In OER four electron transfer mechanism is used instead of two electron transfer mechanism. Among the prepared samples hybrid of WC with UiO-66 i.ie., WC 6 shows the least over potential of (152) at 10 mA/cm^2 current density in 1 M alkaline electrolyte. The other prepared hybrids i.e., WC 1, WC 2, WC 3, WC 4, WC 5, WC 6, pure WC, Pure UIO-66, and pure PBNPs required an over potential of (192), (190), (178), (173), (185), (152), (223), (350), and (360) respectively to attain a current density in the same electrolyte solution as shown in the **figure (c, d)**. WC 6 shows better activity among all the catalyst because of the presence of UiO-66 which has high stability, highly porous in nature and a high surface area than that of PBNPs and WC. Moreover, the enhanced catalytic activity of all the hybrids as compared to the pure compounds is also because of the synergistic effects of both the compounds in the hybrids. The overall properties of the hybrids are enhanced, and, in the result, the catalytic activity is also improved. The better OER catalytic performance of WC 1, WC 2, and WC 3 as compared to pure WC and pure PBNPs is also because of the synergistic properties of both the materials in the hybrids. Conductive properties and enhanced surface area increases the charge transfer and as result the activity is enhanced.

The Tafel plot of all the prepared samples are shown in **figure (g, h)**. As can be seen in the figure that WC 6 has the smallest Tafel slope of 63 mV/dec and the lower the Tafel slope the better the activity of that catalyst. This low Tafel slope indicates that WC6 has a fast oxygen evolution charge transfer ability with enhanced reaction kinetics for electrocatalytic OER, this statement is verified from the EIS spectroscopy as shown in figure. The Tafel slope of all other hybrids i.e., pure WC, pure PBNPs, Pure UiO-66, WC 1, WC 2, WC 3, WC 4, and WC 5 are (159mV/dec), (187), (196), (136), (132), (102), (105), and (113mV/dec) respectively. The Tafel slope of pure WC suggests that the adsorption rate of hydroxyl ion on the surface of catalyst is poor, but with the addition of PBNPs and UiO-66 the OER activity is enhanced giving us low Tafel slope values. This phenomenon is because of the absorbed oxygen with the cation sites of transition metals. In the hybrid the heterostructure of Fe, W, and Zr speed up the electron transport and as a result electrochemical performance is improved as compared to that of pure compounds. The overpotential of some hybrids are given in **table 5** for comparison with the work of this paper.

Table 5: Comparison of some catalyst with this research.

Catalyst	Reaction Type	Electrolyte	Tafel slope	Over potential	Current density (mA/cm^2)	Reference
WC@UiO66	HER OER	1 M KOH 1 M KOH		104 152	10	This work
W_2N/WC	HER OER	1 M KOH 1 M KOH	47.4 94	148.5 320	10	[171]
WCx/C	HER	0.5 M H2SO4	85	264	10	[172]
W_2C-HS	HER	0.5 M H2SO4	67.8	153	10	[173]
WC- Nickle doping	OER	1 M KOH	93	378	10	[174]

Co/W-C@NCNSs	OER	1 M KOH	75.5	323	10	[175]
W_6Co_6C@NC	OER	1 M KOH	54	286	10	[176]

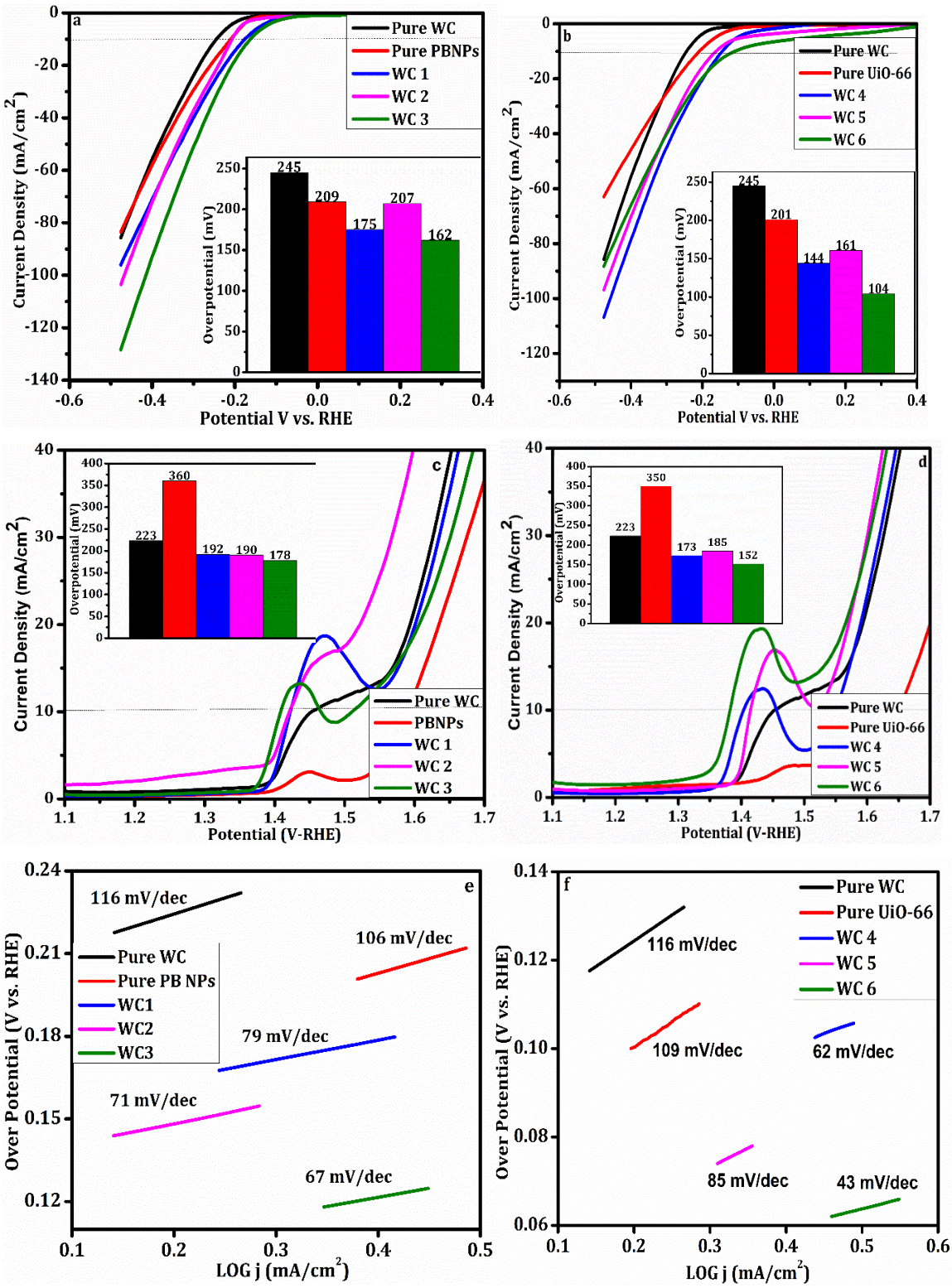
a
Pure WC
Pure PBNPs
WC 1
WC 2
WC 3
Current Density (mA/cm2)
Potential V vs. RHE
Overpotential (mV)
245
209
175
207
162
b
Pure WC
Pure UiO-66
WC 4
WC 5
WC 6
Current Density (mA/cm2)
Potential V vs. RHE
Overpotential (mV)
245
201
144
161
104
c
Pure WC
PBNPs
WC 1
WC 2
WC 3
Current Density (mA/cm2)
Potential (V-RHE)
Overpotential (mV)
223
360
192
190
178
d
Pure WC
Pure UiO-66
WC 4
WC 5
WC 6
Current Density (mA/cm2)
Potential (V-RHE)
Overpotential (mV)
223
350
173
185
152
e
116 mV/dec
106 mV/dec
79 mV/dec
71 mV/dec
67 mV/dec
Pure WC
Pure PB NPs
WC1
WC2
WC3
Over Potential (V vs. RHE)
LOG j (mA/cm2)
f
116 mV/dec
109 mV/dec
62 mV/dec
85 mV/dec
43 mV/dec
Pure WC
Pure UiO-66
WC 4
WC 5
WC 6
Over Potential (V vs. RHE)
LOG j (mA/cm2)

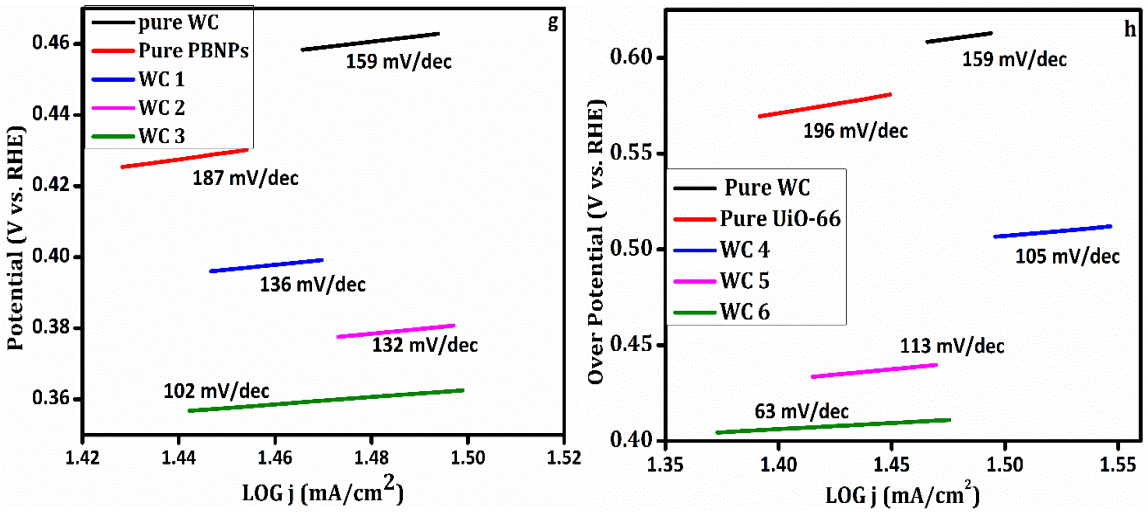

Figure 16:(a, b) LSV curves for HER, (c, d) LSV curves for OER. (e, f) Tafel plots of HER, (g, h) Tafel Plots of OER.

4.4.3 Cyclic Voltametery:

To study the relation between current density over a range of voltage (0 to 600mV) cyclic voltametery of all the fabricated catalysts was performed at a scan rate of 100mV/s as shown in the **figure 17 (a, b).** The graph of CV gives information about the thermodynamics of the oxidation and reduction reactions as well as about the kinetics model of the electron transfer reactions. As can be seen form the figure that two distinct redox peaks are present in the CV graph correspond to the oxidation peak above and the reduction peak below [177]. From the CV of a catalyst, we can find out area under the curve and from that electrochemical active surface area (ESCA) is determined. **Figure 17 (c)** shows the CV graph of WC 6 at different scan rates from 0 to 50 mV/s. in the given potential range two redox peaks are shown. Transfer of charge take place between the redox sites through WC 6, and ions are transferred through the electrode's pores with no change in the structure. From the profile of CV, it is clear that it stays consistent with gradual increase in the area as the scan rate is increased which shows strong cyclic stability, better electrocatalytic efficiency, and low resistance of the catalyst. By increasing the scan rate, the impedance of the absorber layer is decreased, resulting in a high current density. As the scan rate increases, the redox peaks increase gradually, indicating that the redox activity is confined to the surface of WC 6, and proving the stability of the catalyst.

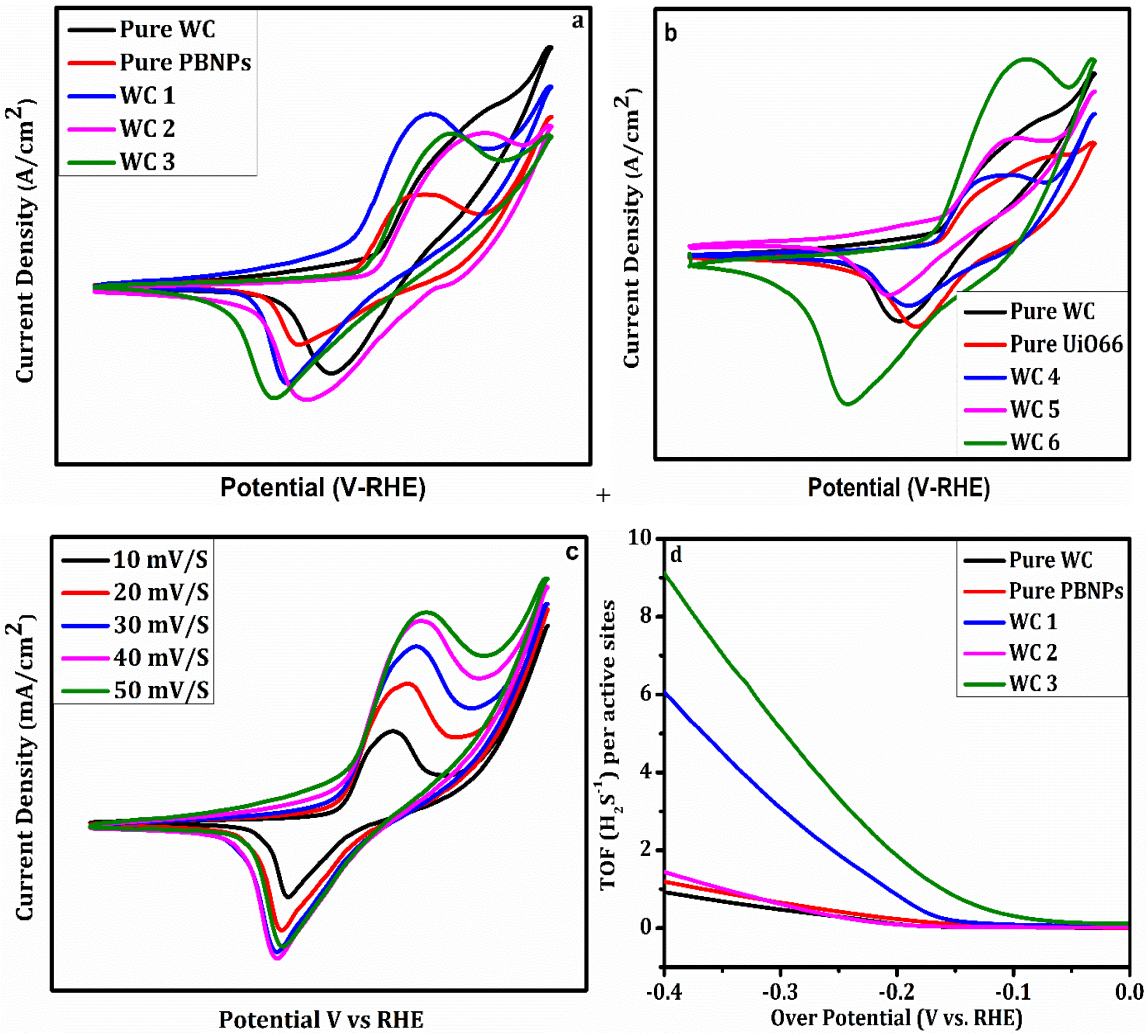
a
Pure WC
Pure PBNPs
WC 1
WC 2
WC 3
Current Density (A/cm2)
Potential (V-RHE)
b
Pure WC
Pure UiO66
WC 4
WC 5
WC 6
Current Density (A/cm2)
Potential (V-RHE)
c
10 mV/S
20 mV/S
30 mV/S
40 mV/S
50 mV/S
Current Density (mA/cm2)
Potential V vs RHE
d
Pure WC
Pure PBNPs
WC 1
WC 2
WC 3
TOF (H2S-1) per active sites
Over Potential (V vs. RHE)

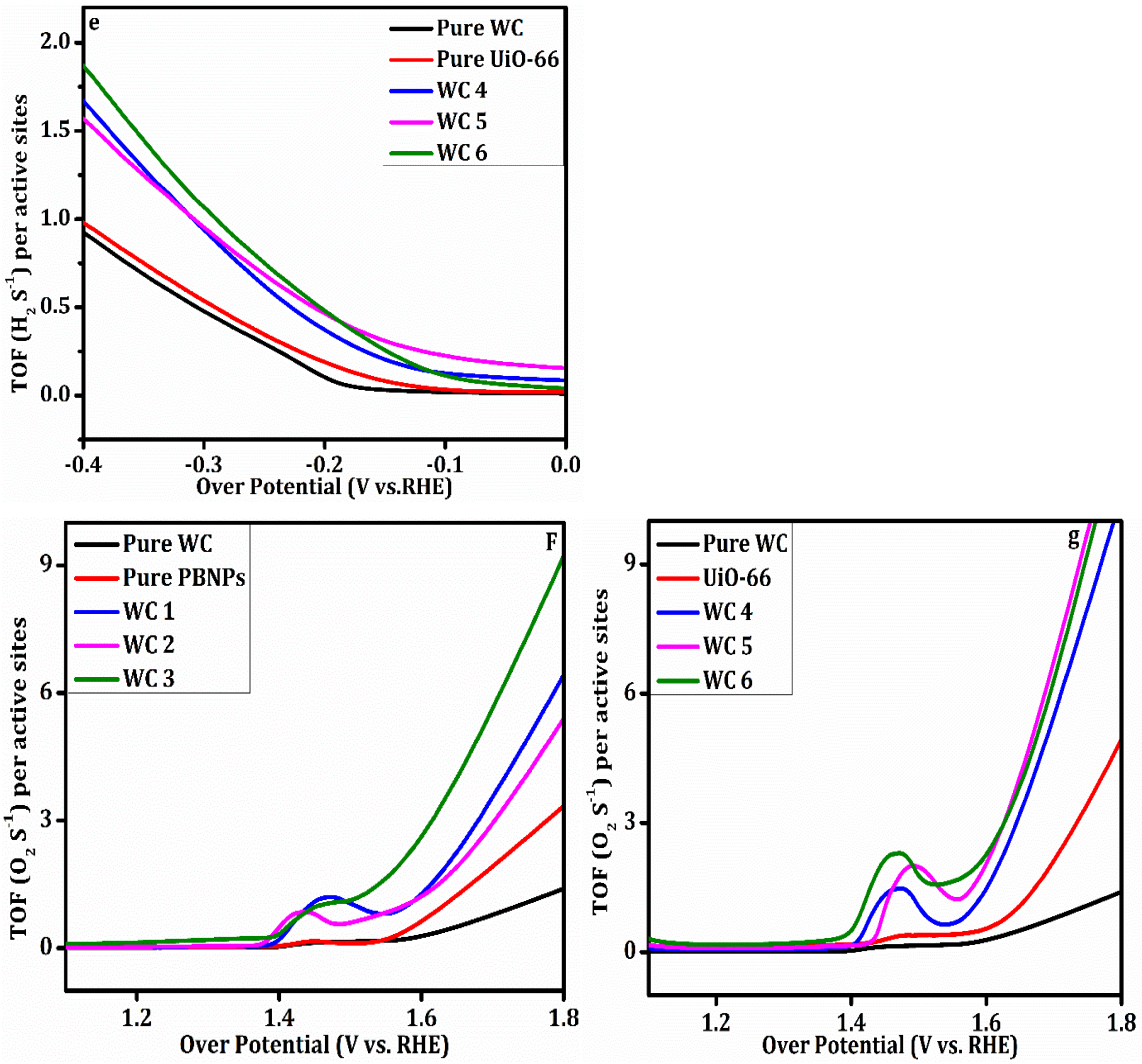

Figure 17:(a) CVs of WC@PBNPs hybrids (b) CVs of WC@UiO-66 hybrids (c) CV curves of WC 6 at different scan rates, (d, e) TOF of the hybrids for HER, (f, g) TOF of Hybrids for OER.

4.4.4 Electrochemical Impedance Spectroscopy and Chronopotentiometry:

One of the important parameters to further study about the catalytic activity of fabricated catalyst electrochemical impedance spectroscopy (EIS) is performed. EIS of all the prepared catalysts are shown in the **figure 18 (a, b)** along with the analogues circuit. The test was performed in a frequency range of 200kHz to 0.1Hz in 1 molar alkaline electrolyte. In the Nyquist plot imaginary impedance is given on the y- axis and real impedance is given on the x-axis. EIS is used to find out the charge transfer resistance R_{ct}, polarization resistance R_p, Warburg resistance W (resistance due to electrode to electrolyte interface), and faradic capacitance C_p. the values of the resistance are given in the table. Generally,

from the literature it is studied that small values of R_{ct} have rapid charge transfer ability [178]. Our best catalyst i.e., WC 6 has a small semicircle as compared to other catalysts indicating that this catalyst offers low charge transfer resistance and hence shows good electrocatalytic activity also verified from its Tafel slope values. Values of charge transfer resistance and solution resistance is given in the **table 6**. One of the effective approaches for finding the electrocatalytic performance of a catalyst is to find out electrochemical active surface area (ECSA). The performance of a catalyst is directly proportional to ECSA. The larger the electrochemical active surface area of the catalyst the better will be the performance of that catalyst. ECSA of the catalyst can be find out using the following equation [179].

ECSA = Cp/Cs

In the above equation the value of specific capacitance is constant and given as 40 μF/cm2.

Cp is the electrochemical capacitance, and it is equal to $Cp = A/(2*m*k) (V_2-V_1)$

Here

A is the area under the CV curve and it is determined from the CV curve through origin software.

m is the mass loaded.

k is the scan rate on which experiment is performed here it is 0.05V/s

V_2-V_1 is the final and initial potential here its value is 0.6 V.

The electrochemical active surface area of the prepared catalyst find out is given in the table.

For the practical applications of a catalyst stability or durability of that catalyst is an important parameter. It can be seen by finding the changes in the over potential current density with time using chronopotentiometry. The stability test of WC 6 is performed for 20 h to get chronopotentiometry curve in 1 molar KOH electrolyte solution. From the **figure 18 (c)** it can be seen that the catalyst shows excellent stability with a small drop in

the activity as time passes. This stability is because of the structural properties of the catalyst.

Table 6: Resistance and ECSA of the prepared samples.

Catalyst	Rs	R_{ct}	ECSA
WC	6.1878	2.4108	2170
PBNPs	7.6218	3.8167	1828
UiO-66	3.107	1.9296	2188.36
WC 1	2.1558	1.7712	2694
WC 2	3.264	1.5214	2458.333
WC 3	1.81	1.03	3504.312
WC 4	5.778	0.898	3288.061
WC 5	6.2753	0.289	3111.37
WC 6	5.996	0.257	6431.719

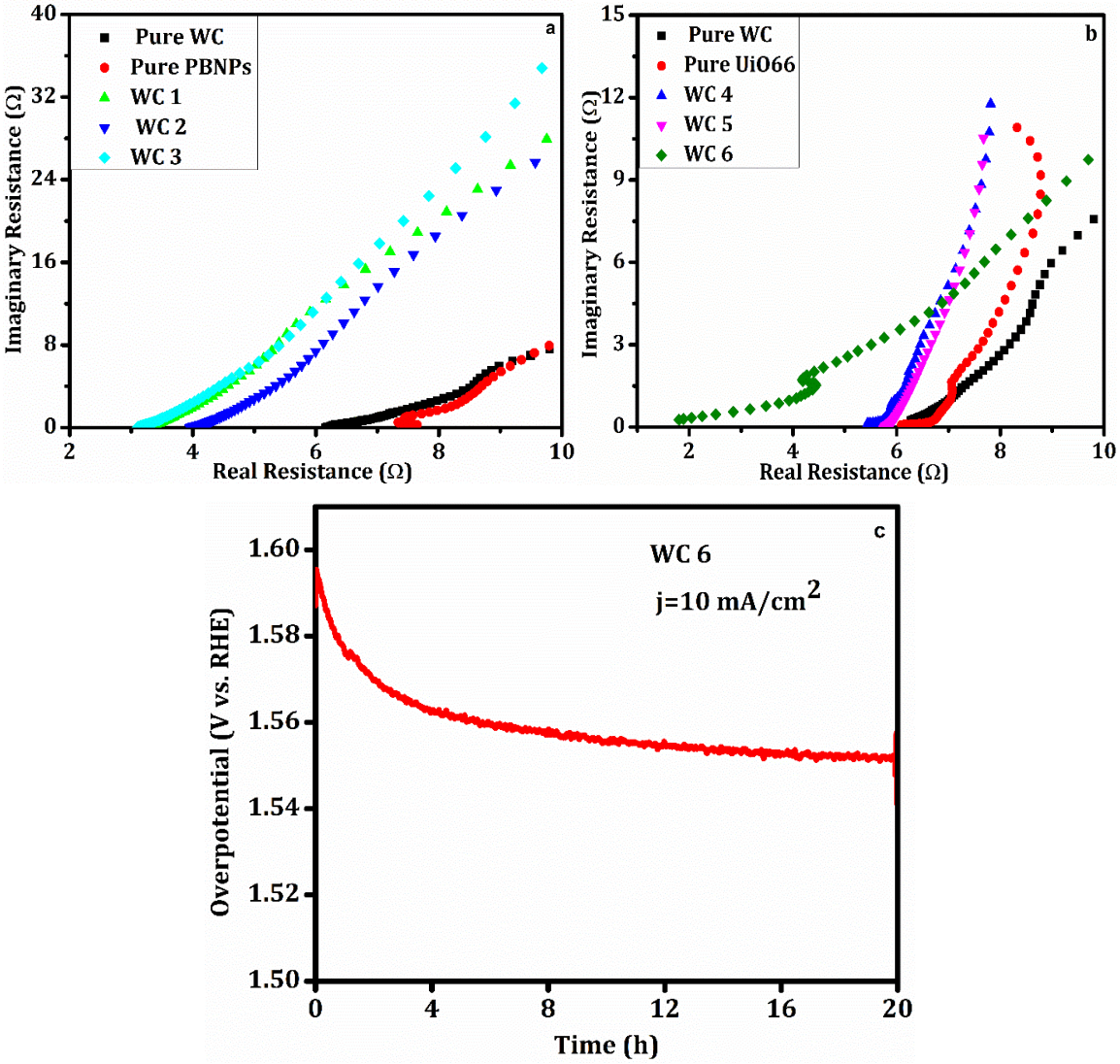

Figure 18:(a, b) EIS of the prepared samples, (c) Chronopotentiometry of WC 6.

4.5 Proposed Mechanism:

For HER the proposed mechanism will be that of Volmer-Heyrovsky. This can be found out from the Tafel slope values. In the first step an intermediate of H^* is formed from the adsorbed hydrogen on the electrode surface. In the second step a molecule of hydrogen is formed from the electrochemical desorption of hydrogen generated in the first step. The overall mechanism is shown in figure and the corresponding reactions are given as

1. Volmer Reaction

$$H_2O + e^- \rightarrow H^* + OH^-$$

2. Heyrovsky Reaction:

$H_2O + e^- + H^* \rightarrow H_2 + OH^-$

For OER a four-step mechanism is used as shown in the figure the reactions that are taking place are given as

$M + OH^- \rightarrow MOH + e^-$

$MOH + OH^- \rightarrow MO + H_2O + e^-$

$MO + OH^- \rightarrow MOOH + e^-$

$MOOH + OH^- \rightarrow M + O_2 + H_2O + e^-$

Conclusion and Future Prospects:

Summarizing this review, hydrogen can be used as the prime source of energy in the near future as other conventional sources of energy are diminishing at a rapid rate. To address this issue, many researchers showcase their skills and prepare different catalysts that can be used to enhance the production of hydrogen through electrocatalytic water splitting. Because of its low cost, high stability, the greater number of operational sites, and catalytically active nature, transition metal-based catalysts are the most effective catalysts for hydrogen production. Among the transition metal catalysts, tungsten carbide and its hybrids show the most promising results. The conclusions that have been made from all this research about WC and its hybrids can be summarized as

1. The purity of the synthesized WC is strongly dependent on the route of the synthesis method. The smallest over potential observed for tungsten carbide hybrid is observed to be 51 mV which is prepared by sample pyrolysis technique as shown in Table 2.
2. The catalytic activity of the WC can be improved up to a great extent by making hybrids of it with different MOFs and materials having large surface areas.
3. The catalytic activity of WC and its hybrids are like that of platinum metal with a low Tafel slope and low overpotential for both HER and OER. However, the activity is greater in HER as compared to OER in alkaline media.
4. From the above research and evaluation, it is concluded that the WC prepared by Lulu Qiao has the best activity by providing the lowest overpotential of 98 mV and Tafel slope of 54 mV/dec for a typical hydrogen evolution reaction.

Although a lot of progress has been made in the synthesis of effective catalysts and researchers have succeeded in the preparation of WC and its different hybrids, which shows the similar activity as benchmark catalysts, there are many challenges and issues that still need to be addressed before the commercialization of water splitting process for hydrogen production using WC as electrocatalyst. The study of active sites of WC and other transition metal catalysts for HER mechanism needs attention and requires immediate research. Stoichiometric study of tungsten and carbon for HER reactions is also an area

that needs improvement. Enhancement in the catalyst nanostructure is also needed for a larger active surface area and for the study of synergistic effects. Another region that needs to be addressed is the preparation of hybrids of WC with conductive materials for better transmission of charge carriers.

References:

[1] M. Ali, E. Pervaiz, T. Noor, O. Rabi, R. Zahra, and M. J. I. J. o. E. R. Yang, "Recent advancements in MOF-based catalysts for applications in electrochemical and photoelectrochemical water splitting: A review," vol. 45, no. 2, pp. 1190-1226, 2021.

[2] R. A. D. Y. A. J. E. ATALAN, E. NUMERICAL ADVANCES IN SCIENCE, and TECHNOLOGY, "THE COMPARISON OF ENERGY RESOURCES IN THE CONTEXT OF GLOBAL ENERGY SUPPLY SECURITY," p. 3, 2021.

[3] U. Abdullah, M. Ali, E. Pervaiz, and R. J. I. J. o. E. R. Khosa, "An inclusive perspective on the recent development of tungsten-based catalysts for overall water-splitting: A review," 2022.

[4] U. Abdullah, M. Ali, and E. Pervaiz, "An Inclusive Review on Recent Advancements of Cadmium Sulfide Nanostructures and its Hybrids for Photocatalytic and Electrocatalytic Applications," *Molecular Catalysis,* vol. 508, 2021.

[5] R. Moliner, M. Lázaro, and I. J. I. j. o. h. e. Suelves, "Analysis of the strategies for bridging the gap towards the Hydrogen Economy," vol. 41, no. 43, pp. 19500-19508, 2016.

[6] S. Singh *et al.*, "Hydrogen: A sustainable fuel for future of the transport sector," *Renewable and Sustainable Energy Reviews*, vol. 51, pp. 623-633, 2015.

[7] R. Asahi, T. Morikawa, T. Ohwaki, K. Aoki, and Y. J. s. Taga, "Visible-light photocatalysis in nitrogen-doped titanium oxides," vol. 293, no. 5528, pp. 269-271, 2001.

[8] G. R. Bamwenda, S. Tsubota, T. Nakamura, M. J. J. o. P. Haruta, and P. A. Chemistry, "Photoassisted hydrogen production from a water-ethanol solution: a comparison of activities of Au□ TiO2 and Pt□ TiO2," vol. 89, no. 2, pp. 177-189, 1995.

[9] J.-M. J. C. t. Herrmann, "Heterogeneous photocatalysis: fundamentals and applications to the removal of various types of aqueous pollutants," vol. 53, no. 1, pp. 115-129, 1999.

[10] N. Meng, M. Leung, K. Sumathy, and D. Leung, "Water electrolysis-a bridge between renewable resources and hydrogen," in *Proceedings of the international hydrogen energy forum*, 2004, vol. 1.

[11] M. Allen *et al.*, "Technical Summary: Global warming of 1.5 C. An IPCC Special Report on the impacts of global warming of 1.5 C above pre-industrial levels and related global greenhouse gas emission pathways, in the context of strengthening the global response to the threat of climate change, sustainable development, and efforts to eradicate poverty," 2019.

[12] I. Dincer and C. J. I. J. o. E. R. Acar, "A review on clean energy solutions for better sustainability," vol. 39, no. 5, pp. 585-606, 2015.

[13] N. Panwar, S. Kaushik, S. J. R. Kothari, and s. e. reviews, "Role of renewable energy sources in environmental protection: A review," vol. 15, no. 3, pp. 1513-1524, 2011.

[14] A. M. Abdalla *et al.*, "Hydrogen production, storage, transportation and key challenges with applications: A review," vol. 165, pp. 602-627, 2018.

[15] C. Acar and I. J. J. o. c. p. Dincer, "Review and evaluation of hydrogen production options for better environment," vol. 218, pp. 835-849, 2019.

[16] B. Johnston, M. C. Mayo, and A. J. T. Khare, "Hydrogen: the energy source for the 21st century," vol. 25, no. 6, pp. 569-585, 2005.

[17] B. You and Y. J. A. o. c. r. Sun, "Innovative strategies for electrocatalytic water splitting," vol. 51, no. 7, pp. 1571-1580, 2018.

[18] T. Hisatomi and K. J. N. C. Domen, "Reaction systems for solar hydrogen production via water splitting with particulate semiconductor photocatalysts," vol. 2, no. 5, pp. 387-399, 2019.

[19] M. J. I. J. o. H. E. Amoretti, "Towards a peer-to-peer hydrogen economy framework," vol. 36, no. 11, pp. 6376-6386, 2011.

[20] R. Zahra *et al.*, "A review on nickel cobalt sulphide and their hybrids: Earth abundant, pH stable electro-catalyst for hydrogen evolution reaction," vol. 45, no. 46, pp. 24518-24543, 2020.

[21] J. E. Lee *et al.*, "Mini review on H2 production from electrochemical water splitting according to special nanostructured morphology of electrocatalysts," vol. 308, p. 122048, 2022.

[22] X. Zou and Y. Zhang, "Noble metal-free hydrogen evolution catalysts for water splitting," *Chem Soc Rev,* vol. 44, no. 15, pp. 5148-80, Aug 7 2015.

[23] O. Rabi, E. Pervaiz, R. Zahra, M. Ali, and M. B. K. Niazi, "An inclusive review on the synthesis of molybdenum carbide and its hybrids as catalyst for electrochemical water splitting," *Molecular Catalysis,* vol. 494, 2020.

[24] M. Ni, M. K. H. Leung, D. Y. C. Leung, and K. Sumathy, "A review and recent developments in photocatalytic water-splitting using TiO2 for hydrogen production," *Renewable and Sustainable Energy Reviews,* vol. 11, no. 3, pp. 401-425, 2007.

[25] Y. Choquette, L. Brossard, A. Lasia, and H. J. J. o. T. E. S. Menard, "Study of the kinetics of hydrogen evolution reaction on raney nickel composite-coated electrode by AC impedance technique," vol. 137, no. 6, p. 1723, 1990.

[26] A. Lasia, A. J. J. o. e. c. Rami, and i. electrochemistry, "Kinetics of hydrogen evolution on nickel electrodes," vol. 294, no. 1-2, pp. 123-141, 1990.

[27] Y. Cao, L. Shen, X. Hu, Z. Du, and L. J. C. E. J. Jiang, "Low temperature desulfurization on Co-doped α-FeOOH: Tailoring the phase composition and creating the defects," vol. 306, pp. 124-130, 2016.

[28] C. Lei *et al.*, "Charge engineering of Mo2C@ defect-rich N-doped carbon nanosheets for efficient electrocatalytic H2 evolution," vol. 11, no. 1, pp. 1-10, 2019.

[29] Z. Shi *et al.*, "Phosphorus-Mo 2 C@ carbon nanowires toward efficient electrochemical hydrogen evolution: composition, structural and electronic regulation," vol. 10, no. 5, pp. 1262-1271, 2017.

[30] B. L. Phoon, C. W. Lai, J. C. Juan, P.-L. Show, and G.-T. J. I. J. o. H. E. Pan, "Recent developments of strontium titanate for photocatalytic water splitting application," vol. 44, no. 28, pp. 14316-14340, 2019.

[31] Z. Luo, T. Wang, and J. J. C. S. R. Gong, "Single-crystal silicon-based electrodes for unbiased solar water splitting: current status and prospects," vol. 48, no. 7, pp. 2158-2181, 2019.

[32] M. Shen, N. Bennett, Y. Ding, and K. J. i. j. o. h. e. Scott, "A concise model for evaluating water electrolysis," vol. 36, no. 22, pp. 14335-14341, 2011.

[33] S. Anantharaj and S. J. S. Noda, "Amorphous catalysts and electrochemical water splitting: an untold story of harmony," vol. 16, no. 2, p. 1905779, 2020.

[34] L. Zhang *et al.*, "Recent advances in 1D electrospun nanocatalysts for electrochemical water splitting," vol. 2, no. 2, p. 2000048, 2021.

[35] H. Zhang, A. W. Maijenburg, X. Li, S. L. Schweizer, and R. B. J. A. F. M. Wehrspohn, "Bifunctional heterostructured transition metal phosphides for efficient electrochemical water splitting," vol. 30, no. 34, p. 2003261, 2020.

[36] Z. Chen, X. Duan, W. Wei, S. Wang, and B.-J. J. N. E. Ni, "Iridium-based nanomaterials for electrochemical water splitting," vol. 78, p. 105270, 2020.

[37] J. Joy, J. Mathew, and S. C. J. I. J. o. h. e. George, "Nanomaterials for photoelectrochemical water splitting–review," vol. 43, no. 10, pp. 4804-4817, 2018.

[38] A. Juliya, V. A. Mujeeb, K. Sreenivasan, K. J. J. o. P. Muraleedharan, and Photobiology, "Enhanced H2 evolution via photocatalytic water splitting using mesoporous TiO2/RuO2/CuO ternary nanomaterial," vol. 8, p. 100076, 2021.

[39] P. Sahu, V. Wagh, S. Zodge, S. Patil, K. J. J. f. R. Suryawanshi, and Volume, "Hydrogen Generation from Waste Water by using Solar Energy," vol. 3, no. 11, 2018.

[40] J. Joy, J. Mathew, and S. C. George, "Nanomaterials for photoelectrochemical water splitting – review," *International Journal of Hydrogen Energy*, vol. 43, no. 10, pp. 4804-4817, 2018.

[41] G. J. A. C. A. G. Colón, "Towards the hydrogen production by photocatalysis," vol. 518, pp. 48-59, 2016.

[42] K. J. J. o. P. Maeda and P. C. P. Reviews, "Photocatalytic water splitting using semiconductor particles: history and recent developments," vol. 12, no. 4, pp. 237-268, 2011.

[43] N. Fajrina and M. Tahir, "A critical review in strategies to improve photocatalytic water splitting towards hydrogen production," *International Journal of Hydrogen Energy,* vol. 44, no. 2, pp. 540-577, 2019.

[44] S. H. Jensen, P. H. Larsen, and M. J. I. J. o. H. E. Mogensen, "Hydrogen and synthetic fuel production from renewable energy sources," vol. 32, no. 15, pp. 3253-3257, 2007.

[45] Y. Yan, B. Y. Xia, B. Zhao, and X. Wang, "A review on noble-metal-free bifunctional heterogeneous catalysts for overall electrochemical water splitting," *Journal of Materials Chemistry A,* vol. 4, no. 45, pp. 17587-17603, 2016.

[46] S. Sagadevan, I. Das, P. Singh, and J. Podder, "Synthesis of tungsten carbide nanoparticles by hydrothermal method and its Characterization," *Journal of Materials Science: Materials in Electronics,* vol. 28, no. 1, pp. 1136-1141, 2016.

[47] G. Singla, K. Singh, and O. P. Pandey, "Synthesis of carbon coated tungsten carbide nano powder using hexane as carbon source and its structural, thermal and electrocatalytic properties," *International Journal of Hydrogen Energy,* vol. 40, no. 16, pp. 5628-5637, 2015.

[48] S. Hagege, J. Vicens, G. Nouet, and P. J. P. s. s. Delavignette, "Analysis of structure defects in tungsten carbide," vol. 61, no. 2, pp. 675-687, 1980.

[49] N. J. A. M. Schönberg, "The tungsten carbide and nickel arsenide structures," vol. 2, no. 3, pp. 427-432, 1954.

[50] P. N. Ross Jr and P. J. J. o. c. Stonehart, "The relation of surface structure to the electrocatalytic activity of tungsten carbide," vol. 48, no. 1-3, pp. 42-59, 1977.

[51] G. Wallace, "Synthesis of Carbide Ceramics via Reduction and Carburization of Oxyanions Adsorbed onto an Activated Carbon Matrix," Montana Tech of The University of Montana, 2020.

[52] S. Sagadevan, I. Das, P. Singh, and J. J. J. o. M. S. M. i. E. Podder, "Synthesis of tungsten carbide nanoparticles by hydrothermal method and its Characterization," vol. 28, pp. 1136-1141, 2017.

[53] X. Li, X. Hao, A. Abudula, and G. J. J. o. M. C. A. Guan, "Nanostructured catalysts for electrochemical water splitting: current state and prospects," vol. 4, no. 31, pp. 11973-12000, 2016.

[54] H. Wu, Q. Liu, L. Zhang, Y. Tang, G. Wang, and G. J. A. A. E. M. Mao, "Novel nanostructured WO3@ prussian blue heterojunction photoanodes for efficient photoelectrochemical water splitting," vol. 4, no. 11, pp. 12508-12514, 2021.

[55] M. Zhang *et al.*, "Efficient charge migration in chemically-bonded Prussian blue analogue/CdS with beaded structure for photocatalytic H2 evolution," vol. 1, no. 2, pp. 212-220, 2021.

[56] A. Gotoh *et al.*, "Simple synthesis of three primary colour nanoparticle inks of Prussian blue and its analogues," vol. 18, no. 34, p. 345609, 2007.

[57] M. Ali, E. Pervaiz, U. Sikandar, and Y. J. I. J. o. H. E. Khan, "A review on the recent developments in zirconium and carbon-based catalysts for photoelectrochemical water-splitting," vol. 46, no. 35, pp. 18257-18283, 2021.

[58] Y. Feng, Q. Chen, M. Jiang, J. J. I. Yao, and E. C. Research, "Tailoring the properties of UiO-66 through defect engineering: A review," vol. 58, no. 38, pp. 17646-17659, 2019.

[59] B. Feng, H. Wang, D. Wang, H. Yu, Y. Chu, and H.-T. J. N. Fang, "Fabrication of mesoporous metal oxide coated-nanocarbon hybrid materials via a polyol-mediated self-assembly process," vol. 6, no. 23, pp. 14371-14379, 2014.

[60] L. Zeng *et al.*, "A flexible porous carbon nanofibers-selenium cathode with superior electrochemical performance for both Li-Se and Na-Se batteries," vol. 5, no. 4, p. 1401377, 2015.

[61] S. Shiva Kumar, S. U. B. Ramakrishna, S. V. Krishna, K. Srilatha, B. R. Devi, and V. Himabindu, "Synthesis of titanium (IV) oxide composite membrane for hydrogen production through alkaline water electrolysis," *South African Journal of Chemical Engineering,* vol. 25, pp. 54-61, 2018.

[62] S. Shiva Kumar and V. Himabindu, "Hydrogen production by PEM water electrolysis – A review," *Materials Science for Energy Technologies,* vol. 2, no. 3, pp. 442-454, 2019.

[63] K. Zeng and D. Zhang, "Recent progress in alkaline water electrolysis for hydrogen production and applications," *Progress in Energy and Combustion Science,* vol. 36, no. 3, pp. 307-326, 2010.

[64] S. S. Kumar, S. Ramakrishna, D. S. Reddy, D. Bhagawan, and V. J. I. J. C. E. P. T. Himabindu, "Synthesis of polysulfone and zirconium oxide coated asbestos composite separators for alkaline water electrolysis," vol. 3, no. 1035, pp. 1-1035, 2017.

[65] M. Ni, M. Leung, and D. Leung, "Technological development of hydrogen production by solid oxide electrolyzer cell (SOEC)," *International Journal of Hydrogen Energy,* vol. 33, no. 9, pp. 2337-2354, 2008.

[66] M. A. Laguna-Bercero, "Recent advances in high temperature electrolysis using solid oxide fuel cells: A review," *Journal of Power Sources,* vol. 203, pp. 4-16, 2012.

[67] F. M. Sapountzi, J. M. Gracia, C. J. Weststrate, H. O. A. Fredriksson, and J. W. Niemantsverdriet, "Electrocatalysts for the generation of hydrogen, oxygen and synthesis gas," *Progress in Energy and Combustion Science,* vol. 58, pp. 1-35, 2017.

[68] A. S. Aricò, S. Siracusano, N. Briguglio, V. Baglio, A. Di Blasi, and V. Antonucci, "Polymer electrolyte membrane water electrolysis: status of technologies and potential applications in combination with renewable power sources," *Journal of Applied Electrochemistry,* vol. 43, no. 2, pp. 107-118, 2012.

[69] M. Carmo, D. L. Fritz, J. Mergel, and D. Stolten, "A comprehensive review on PEM water electrolysis," *International Journal of Hydrogen Energy,* vol. 38, no. 12, pp. 4901-4934, 2013.

[70] M. Balat, "Potential importance of hydrogen as a future solution to environmental and transportation problems," *International Journal of Hydrogen Energy,* vol. 33, no. 15, pp. 4013-4029, 2008.

[71] S. J. J. o. E. C. Trasatti, "Water electrolysis: who first?," vol. 476, no. 1, pp. 90-91, 1999.

[72] S. Marini *et al.,* "Advanced alkaline water electrolysis," *Electrochimica Acta,* vol. 82, pp. 384-391, 2012.

[73] A. Kadier, Y. Simayi, P. Abdeshahian, N. F. Azman, K. Chandrasekhar, and M. S. Kalil, "A comprehensive review of microbial electrolysis cells (MEC) reactor designs and configurations for sustainable hydrogen gas production," *Alexandria Engineering Journal,* vol. 55, no. 1, pp. 427-443, 2016.

[74] N. K. Rathinam, R. K. Sani, and D. Salem, "Rewiring extremophilic electrocatalytic processes for production of biofuels and value-added compounds from lignocellulosic biomass," in *Extremophilic Microbial Processing of Lignocellulosic Feedstocks to Biofuels, Value-Added Products, and Usable Power*: Springer, 2018, pp. 229-245.

[75] H. Liu, S. Grot, B. E. J. E. s. Logan, and technology, "Electrochemically assisted microbial production of hydrogen from acetate," vol. 39, no. 11, pp. 4317-4320, 2005.

[76] A. Brisse, J. Schefold, and M. Zahid, "High temperature water electrolysis in solid oxide cells," *International Journal of Hydrogen Energy,* vol. 33, no. 20, pp. 5375-5382, 2008.

[77] W. Xu and K. Scott, "The effects of ionomer content on PEM water electrolyser membrane electrode assembly performance," *International Journal of Hydrogen Energy,* vol. 35, no. 21, pp. 12029-12037, 2010.

[78] M. Liang, B. Yu, M. Wen, J. Chen, J. Xu, and Y. Zhai, "Preparation of LSM–YSZ composite powder for anode of solid oxide electrolysis cell and its activation mechanism," *Journal of Power Sources,* vol. 190, no. 2, pp. 341-345, 2009.

[79] A. H. Abdol Rahim, A. S. Tijani, S. K. Kamarudin, and S. Hanapi, "An overview of polymer electrolyte membrane electrolyzer for hydrogen production: Modeling and mass transport," *Journal of Power Sources,* vol. 309, pp. 56-65, 2016.

[80] P. Nikolaidis and A. Poullikkas, "A comparative overview of hydrogen production processes," *Renewable and Sustainable Energy Reviews,* vol. 67, pp. 597-611, 2017.

[81] R. Gomez, A. Fernandez-Vega, J. M. Feliu, and A. Aldaz, "Hydrogen evolution on platinum single crystal surfaces: effects of irreversibly adsorbed bismuth and antimony on hydrogen adsorption and evolution on platinum (100)," *The Journal of Physical Chemistry,* vol. 97, no. 18, pp. 4769-4776, 2002.

[82] H. Minamimoto, R. Osaka, and K. Murakoshi, "In-situ observation of isotopic hydrogen evolution reactions using electrochemical mass spectroscopy to evaluate surface morphological effect," *Electrochimica Acta*, vol. 304, pp. 87-93, 2019.

[83] E. Skúlason *et al.*, "Density functional theory calculations for the hydrogen evolution reaction in an electrochemical double layer on the Pt (111) electrode," vol. 9, no. 25, pp. 3241-3250, 2007.

[84] D. Alba-Molina *et al.*, "Tailoring the ORR and HER electrocatalytic performances of gold nanoparticles through metal–ligand interfaces," vol. 7, no. 35, pp. 20425-20434, 2019.

[85] Y. Guo *et al.*, "Nanoarchitectonics for transition-metal-sulfide-based electrocatalysts for water splitting," vol. 31, no. 17, p. 1807134, 2019.

[86] C. G. Morales-Guio, L.-A. Stern, and X. J. C. S. R. Hu, "Nanostructured hydrotreating catalysts for electrochemical hydrogen evolution," vol. 43, no. 18, pp. 6555-6569, 2014.

[87] H. Ahmad, S. K. Kamarudin, L. J. Minggu, and M. Kassim, "Hydrogen from photo-catalytic water splitting process: A review," *Renewable and Sustainable Energy Reviews*, vol. 43, pp. 599-610, 2015.

[88] A. Franco, M. Cano, J. J. Giner-Casares, E. Rodríguez-Castellón, R. Luque, and A. R. J. C. C. Puente-Santiago, "Boosting the electrochemical oxygen reduction activity of hemoglobin on fructose@ graphene-oxide nanoplatforms," vol. 55, no. 32, pp. 4671-4674, 2019.

[89] F. Safizadeh, E. Ghali, and G. Houlachi, "Electrocatalysis developments for hydrogen evolution reaction in alkaline solutions – A Review," *International Journal of Hydrogen Energy*, vol. 40, no. 1, pp. 256-274, 2015.

[90] Y. Zheng, Y. Jiao, M. Jaroniec, and S. Z. J. A. C. I. E. Qiao, "Advancing the electrochemistry of the hydrogen-evolution reaction through combining experiment and theory," vol. 54, no. 1, pp. 52-65, 2015.

[91] N. Han, P. Liu, J. Jiang, L. Ai, Z. Shao, and S. J. J. o. M. C. A. Liu, "Recent advances in nanostructured metal nitrides for water splitting," vol. 6, no. 41, pp. 19912-19933, 2018.

[92] L. Li, P. Wang, Q. Shao, and X. J. C. S. R. Huang, "Metallic nanostructures with low dimensionality for electrochemical water splitting," vol. 49, no. 10, pp. 3072-3106, 2020.

[93] G. Yilmaz, C. F. Tan, Y. F. Lim, and G. W. J. A. E. M. Ho, "Pseudomorphic transformation of interpenetrated prussian blue analogs into defective nickel iron selenides for enhanced electrochemical and photo-electrochemical water splitting," vol. 9, no. 1, p. 1802983, 2019.

[94] J. Zhu, L. Hu, P. Zhao, L. Y. S. Lee, and K.-Y. J. C. r. Wong, "Recent advances in electrocatalytic hydrogen evolution using nanoparticles," vol. 120, no. 2, pp. 851-918, 2019.

[95] M. Boudart, *Kinetics of chemical processes: butterworth-heinemann series in chemical engineering*. Elsevier, 2014.

[96] M. J. C. r. Boudart, "Turnover rates in heterogeneous catalysis," vol. 95, no. 3, pp. 661-666, 1995.

[97] H. Jin *et al.*, "Emerging two-dimensional nanomaterials for electrocatalysis," vol. 118, no. 13, pp. 6337-6408, 2018.

[98] S. Trasatti and O. J. J. o. E. C. Petrii, "Real surface area measurements in electrochemistry," vol. 327, no. 1-2, pp. 353-376, 1992.

[99] N. Han *et al.*, "Nitrogen-doped tungsten carbide nanoarray as an efficient bifunctional electrocatalyst for water splitting in acid," vol. 9, no. 1, pp. 1-10, 2018.

[100] S. Lu *et al.*, "Boosting oxygen evolution through phase and electronic modulation of highly dispersed tungsten carbide with nickel doping," *J Colloid Interface Sci*, vol. 585, pp. 258-266, Mar 2021.

[101] S. Zhang *et al.*, "In situ interfacial engineering of nickel tungsten carbide Janus structures for highly efficient overall water splitting," *Science Bulletin*, vol. 65, no. 8, pp. 640-650, 2020.

[102] J. Chen, B. Ren, H. Cui, and C. Wang, "Constructing Pure Phase Tungsten-Based Bimetallic Carbide Nanosheet as an Efficient Bifunctional Electrocatalyst for Overall Water Splitting," *Small*, vol. 16, no. 23, p. e1907556, Jun 2020.

[103] L. Wang *et al.*, "Tuning d-band center of tungsten carbide via Mo doping for efficient hydrogen evolution and Zn–H2O cell over a wide pH range," *Nano Energy,* vol. 74, 2020.

[104] Y. Ling *et al.*, "Tungsten Carbide Hollow Microspheres with Robust and Stable Electrocatalytic Activity toward Hydrogen Evolution Reaction," *ACS Omega,* vol. 4, no. 2, pp. 4185-4191, Feb 28 2019.

[105] Y. Chen, Y. Zheng, X. Yue, and S. Huang, "Hydrogen evolution reaction in full pH range on nickel doped tungsten carbide nanocubes as efficient and durable non-precious metal electrocatalysts," *International Journal of Hydrogen Energy,* vol. 45, no. 15, pp. 8695-8702, 2020.

[106] Y. T. Xu *et al.*, "Cage-Confinement Pyrolysis Route to Ultrasmall Tungsten Carbide Nanoparticles for Efficient Electrocatalytic Hydrogen Evolution," *J Am Chem Soc,* vol. 139, no. 15, pp. 5285-5288, Apr 19 2017.

[107] Y. Wang *et al.*, "Scalable processing hollow tungsten carbide spherical superstructure as an enhanced electrocatalyst for hydrogen evolution reaction over a wide pH range," *Electrochimica Acta,* vol. 319, pp. 775-782, 2019.

[108] S. C. Abbas *et al.*, "Novel strongly coupled tungsten-carbon-nitrogen complex for efficient hydrogen evolution reaction," *International Journal of Hydrogen Energy,* vol. 43, no. 1, pp. 16-23, 2018.

[109] E. H. Ang *et al.*, "Highly Efficient and Stable Hydrogen Production in All pH Range by Two-Dimensional Structured Metal-Doped Tungsten Semicarbides," *Research (Wash D C),* vol. 2019, p. 4029516, 2019.

[110] S. Xu, S. Chu, L. Yang, Y. Chen, Z. Wang, and C. Jiang, "Tungsten nitride/carbide nanocomposite encapsulated in nitrogen-doped carbon shell as an effective and durable catalyst for hydrogen evolution reaction," *New Journal of Chemistry,* vol. 42, no. 24, pp. 19557-19563, 2018.

[111] B. Ren, D. Li, Q. Jin, H. Cui, and C. Wang, "Novel porous tungsten carbide hybrid nanowires on carbon cloth for high-performance hydrogen evolution," *Journal of Materials Chemistry A,* vol. 5, no. 25, pp. 13196-13203, 2017.

[112] H. Jin, J. Chen, S. Mao, and Y. Wang, "Transition Metal Induced the Contraction of Tungsten Carbide Lattice as Superior Hydrogen Evolution Reaction Catalyst," *ACS Appl Mater Interfaces,* vol. 10, no. 26, pp. 22094-22101, Jul 5 2018.

[113] M. Zeng *et al.*, "2D WC single crystal embedded in graphene for enhancing hydrogen evolution reaction," *Nano Energy,* vol. 33, pp. 356-362, 2017.

[114] W. F. Chen *et al.*, "Tungsten carbide-nitride on graphene nanoplatelets as a durable hydrogen evolution electrocatalyst," *ChemSusChem,* vol. 7, no. 9, pp. 2414-8, Sep 2014.

[115] Y. Yan *et al.*, "Nano-tungsten carbide decorated graphene as co-catalysts for enhanced hydrogen evolution on molybdenum disulfide," *Chemical Communications,* vol. 49, no. 43, 2013.

[116] Y. Yan *et al.*, "Template-free pseudomorphic synthesis of tungsten carbide nanorods," *Small,* vol. 8, no. 21, pp. 3350-6, Nov 5 2012.

[117] J. B. d'Arbigny, G. Taillades, J. Rozière, D. Jones, and M. J. E. T. Marrony, "High surface area tungsten carbide with novel architecture and high electrochemical stability," vol. 41, no. 1, p. 1207, 2011.

[118] L. Xiong, L. Zheng, C. Liu, L. Jin, Q. Liu, and J. J. J. o. T. E. S. Xu, "Tungsten carbide microspheres with high surface area as platinum catalyst supports for enhanced electrocatalytic activity," vol. 162, no. 4, p. F468, 2015.

[119] Y. Wang, S. Song, P. K. Shen, C. Guo, and C. M. J. J. o. M. C. Li, "Nanochain-structured mesoporous tungsten carbide and its superior electrocatalysis," vol. 19, no. 34, pp. 6149-6153, 2009.

[120] G. Boopathy, M. Govindasamy, M. Nazari, S.-F. Wang, and M. J. J. o. T. E. S. Umapathy, "Facile synthesis of tungsten carbide nanosheets for trace level detection of toxic mercury ions in biological and contaminated sewage water samples: an electrocatalytic approach," vol. 166, no. 10, p. B761, 2019.

[121] Y. Wang, S. Song, V. Maragou, P. K. Shen, and P. J. A. C. B. E. Tsiakaras, "High surface area tungsten carbide microspheres as effective Pt catalyst support for oxygen reduction reaction," vol. 89, no. 1-2, pp. 223-228, 2009.

[122] J. Gao, S. Wu, J. Chen, Y. Li, and G. J. E. A. Li, "Mesoporous tungsten carbide nanoslices with pure phase and superior electrocatalysis," vol. 222, pp. 728-734, 2016.

[123] F. Medeiros *et al.*, "Synthesis of tungsten carbide through gas–solid reaction at low temperatures," vol. 315, no. 1-2, pp. 58-62, 2001.

[124] J. Ma and S. G. Zhu, "Direct solid-state synthesis of tungsten carbide nanoparticles from mechanically activated tungsten oxide and graphite," *International Journal of Refractory Metals and Hard Materials*, vol. 28, no. 5, pp. 623-627, 2010.

[125] M. Islam and R. Martinez-Duarte, "A sustainable approach for tungsten carbide synthesis using renewable biopolymers," *Ceramics International*, vol. 43, no. 13, pp. 10546-10553, 2017.

[126] K.-F. Wang, G.-D. Sun, Y.-D. Wu, and G.-H. Zhang, "Fabrication of ultrafine and high-purity tungsten carbide powders via a carbothermic reduction–carburization process," *Journal of Alloys and Compounds*, vol. 784, pp. 362-369, 2019.

[127] A. T. Garcia-Esparza, D. Cha, Y. Ou, J. Kubota, K. Domen, and K. Takanabe, "Tungsten carbide nanoparticles as efficient cocatalysts for photocatalytic overall water splitting," *ChemSusChem*, vol. 6, no. 1, pp. 168-81, Jan 2013.

[128] R. Koc and S. K. J. J. o. t. E. C. S. Kodambaka, "Tungsten carbide (WC) synthesis from novel precursors," vol. 20, no. 11, pp. 1859-1869, 2000.

[129] J. Hojo, T. Oku, and A. J. J. o. t. L. C. M. Kato, "Tungsten carbide powders produced by the vapor phase reaction of the WCl6-CH4-H2 system," vol. 59, no. 1, pp. 85-95, 1978.

[130] M. Fitzsimmons, V. K. J. S. Sarin, and C. Technology, "Comparison of WCl6-CH4-H2 and WF6-CH4-H2 systems for growth of WC coatings," vol. 76, pp. 250-255, 1995.

[131] J. Kim and B. J. S. m. Kim, "Synthesis of nanosized tungsten carbide powder by the chemical vapor condensation process," vol. 50, no. 7, pp. 969-972, 2004.

[132] X. Tang, R. Haubner, B. Lux, and B. J. L. J. d. P. I. Kieffer, "Preparation of ultrafine CVD WC powders deposited from WCl6 gas mixtures," vol. 5, no. C5, pp. C5-1013-C5-1020, 1995.

[133] C.-W. Won, B.-S. Chun, and H. J. J. o. m. r. Sohn, "Preparation of ultrafine tungsten carbide powder by CVD method from WCl6–C2H2–H2 mixtures," vol. 8, no. 10, pp. 2702-2708, 1993.

[134] G. Leclercq *et al.*, "Study of the Preparation of Bulk Powder Tungsten Carbides by Temperature Programmed Reaction with CH4+ H2Mixtures," vol. 158, no. 1, pp. 142-169, 1996.

[135] L. Gao and B. J. N. m. Kear, "Low temperature carburization of high surface area tungsten powders," vol. 5, no. 5, pp. 555-569, 1995.

[136] Z. Li *et al.*, "Hollow hemisphere-shaped macroporous graphene/tungsten carbide/platinum nanocomposite as an efficient electrocatalyst for the oxygen reduction reaction," *Electrochimica Acta*, vol. 221, pp. 31-40, 2016.

[137] J. Zhang, J. Chen, Y. Jiang, F. Zhou, G. Wang, and R. Wang, "Tungsten carbide encapsulated in nitrogen-doped carbon with iron/cobalt carbides electrocatalyst for oxygen reduction reaction," *Applied Surface Science*, vol. 389, pp. 157-164, 2016.

[138] F. Sun, X. Chen, and Z. Zhao, "Synthesis of monocrystalline tungsten carbide powder in carbon saturated cobalt melt," *Ceramics International*, vol. 44, no. 7, pp. 8716-8719, 2018.

[139] C. Liu, J. Zhou, Y. Xiao, L. Yang, D. Yang, and D. Zhou, "Structural and electrochemical studies of tungsten carbide/carbon composites for hydrogen evolution," *International Journal of Hydrogen Energy*, vol. 42, no. 50, pp. 29781-29790, 2017.

[140] Y.-J. Ko *et al.*, "Tungsten carbide nanowalls as electrocatalyst for hydrogen evolution reaction: New approach to durability issue," *Applied Catalysis B: Environmental*, vol. 203, pp. 684-691, 2017.

[141] P. Xiao, X. Ge, H. Wang, Z. Liu, A. Fisher, and X. Wang, "Novel Molybdenum Carbide-Tungsten Carbide Composite Nanowires and Their Electrochemical Activation for Efficient and Stable Hydrogen Evolution," *Advanced Functional Materials*, vol. 25, no. 10, pp. 1520-1526, 2015.

[142] A. M. Al-Enizi, R. M. Abdel Hameed, M. M. El-Halwany, M. Bakrey, S. F. Shaikh, and A. Yousef, "Tungsten carbide@graphene nanoflakes: Preparation,

characterization and electrochemical activity for capacitive deionization technology," *J Colloid Interface Sci,* vol. 581, no. Pt A, pp. 112-125, Jan 1 2021.

[143] T. Zhao, J. Gao, J. Wu, P. He, Y. Li, and J. Yao, "Highly Active Cobalt/Tungsten Carbide@N-Doped Porous Carbon Nanomaterials Derived from Metal-Organic Frameworks as Bifunctional Catalysts for Overall Water Splitting," *Energy Technology,* vol. 7, no. 4, 2019.

[144] S. Roy *et al.*, "Mechanistic insights into the promotional effect of Ni substitution in non-noble metal carbides for highly enhanced water splitting," *Applied Catalysis B: Environmental,* vol. 298, 2021.

[145] J. S. Kang *et al.*, "Electrochemical synthesis of nanoporous tungsten carbide and its application as electrocatalysts for photoelectrochemical cells," *Nanoscale,* vol. 9, no. 17, pp. 5413-5424, May 4 2017.

[146] L. Qiao *et al.*, "Achieving electronic structure reconfiguration in metallic carbides for robust electrochemical water splitting," *Journal of Materials Chemistry A,* vol. 8, no. 5, pp. 2453-2462, 2020.

[147] S. Wirth, F. Harnisch, M. Weinmann, and U. Schröder, "Comparative study of IVB–VIB transition metal compound electrocatalysts for the hydrogen evolution reaction," *Applied Catalysis B: Environmental,* vol. 126, pp. 225-230, 2012.

[148] J. Wang, W. Chen, X. Wang, and E. Wang, "N-doped graphene supported W C composite material as an efficient non-noble metal electrocatalyst for hydrogen evolution reaction," *Electrochimica Acta,* vol. 251, pp. 660-671, 2017.

[149] P. Chen, J. Ye, H. Wang, L. Ouyang, and M. Zhu, "Recent progress of transition metal carbides/nitrides for electrocatalytic water splitting," *Journal of Alloys and Compounds,* vol. 883, 2021.

[150] Q. Gong *et al.*, "Ultrasmall and phase-pure W2C nanoparticles for efficient electrocatalytic and photoelectrochemical hydrogen evolution," *Nat Commun,* vol. 7, p. 13216, Oct 18 2016.

[151] P. Bretzler, K. Köhler, A. V. Nikiforov, E. Christensen, R. W. Berg, and N. J. Bjerrum, "Efficient water splitting electrolysis on a platinum-free tungsten carbide electrocatalyst in molten CsH2PO4 at 350–390 °C," *International Journal of Hydrogen Energy,* vol. 45, no. 41, pp. 21262-21272, 2020.

[152] N. Han *et al.*, "Nitrogen-doped tungsten carbide nanoarray as an efficient bifunctional electrocatalyst for water splitting in acid," *Nat Commun,* vol. 9, no. 1, p. 924, Mar 2 2018.

[153] J. Wan *et al.*, "Rapid synthesis of size-tunable transition metal carbide nanodots under ambient conditions," *Journal of Materials Chemistry A*, vol. 7, no. 24, pp. 14489-14495, 2019.

[154] X. F. Lu, L. Yu, J. Zhang, and X. W. D. Lou, "Ultrafine Dual-Phased Carbide Nanocrystals Confined in Porous Nitrogen-Doped Carbon Dodecahedrons for Efficient Hydrogen Evolution Reaction," *Adv Mater,* vol. 31, no. 30, p. e1900699, Jul 2019.

[155] J. Diao *et al.*, "Interfacial Engineering of W2 N/WC Heterostructures Derived from Solid-State Synthesis: A Highly Efficient Trifunctional Electrocatalyst for ORR, OER, and HER," *Adv Mater,* vol. 32, no. 7, p. e1905679, Feb 2020.

[156] T. Wang, X. Wang, Y. Liu, J. Zheng, and X. Li, "A highly efficient and stable biphasic nanocrystalline Ni–Mo–N catalyst for hydrogen evolution in both acidic and alkaline electrolytes," *Nano Energy*, vol. 22, pp. 111-119, 2016.

[157] Z. Chen, M. Qin, P. Chen, B. Jia, Q. He, and X. Qu, "Tungsten carbide/carbon composite synthesized by combustion-carbothermal reduction method as electrocatalyst for hydrogen evolution reaction," *International Journal of Hydrogen Energy*, vol. 41, no. 30, pp. 13005-13013, 2016.

[158] D. Ham, R. Ganesan, and J. Lee, "Tungsten carbide microsphere as an electrode for cathodic hydrogen evolution from water," *International Journal of Hydrogen Energy,* vol. 33, no. 23, pp. 6865-6872, 2008.

[159] J.-F. Lin *et al.*, "Synthesis of tungsten carbide and tungsten disulfide on vertically aligned multi-walled carbon nanotube forests and their application as non-Pt electrocatalysts for the hydrogen evolution reaction," *Journal of Materials Chemistry A*, vol. 3, no. 28, pp. 14609-14616, 2015.

[160] Y. Shen, L. Li, J. Xi, and X. Qiu, "A facile approach to fabricate free-standing hydrogen evolution electrodes: riveting tungsten carbide nanocrystals to graphite felt fabrics by carbon nanosheets," *Journal of Materials Chemistry A*, vol. 4, no. 16, pp. 5817-5822, 2016.

[161] C. Tang, D. Wang, Z. Wu, and B. J. I. J. o. H. E. Duan, "Tungsten carbide hollow microspheres as electrocatalyst and platinum support for hydrogen evolution reaction," vol. 40, no. 8, pp. 3229-3237, 2015.

[162] Y. Zhao, K. Kamiya, K. Hashimoto, and S. Nakanishi, "Hydrogen evolution by tungsten carbonitride nanoelectrocatalysts synthesized by the formation of a tungsten acid/polymer hybrid in situ," *Angew Chem Int Ed Engl*, vol. 52, no. 51, pp. 13638-41, Dec 16 2013.

[163] S. T. Hunt, T. Nimmanwudipong, and Y. Roman-Leshkov, "Engineering non-sintered, metal-terminated tungsten carbide nanoparticles for catalysis," *Angew Chem Int Ed Engl*, vol. 53, no. 20, pp. 5131-6, May 12 2014.

[164] X. Ma, "Advanced Energy Efficiency Technologies for Solar Heating, Cooling and Power Generation," 2019.

[165] M. Zeng *et al.*, "2D WC single crystal embedded in graphene for enhancing hydrogen evolution reaction," vol. 33, pp. 356-362, 2017.

[166] U. Abdullah, M. Ali, and E. J. I. J. o. H. E. Pervaiz, "Cadmium sulfide embedded Prussian Blue as highly active bifunctional electrocatalyst for water-splitting process," vol. 47, no. 49, pp. 21160-21172, 2022.

[167] V. Vinila *et al.*, "XRD studies on nano crystalline ceramic superconductor PbSrCaCuO at different treating temperatures," vol. 2014, 2014.

[168] M. B. Zakaria *et al.*, "Prussian blue derived nanoporous iron oxides as anticancer drug carriers for magnetic-guided chemotherapy," vol. 10, no. 7, pp. 1457-1462, 2015.

[169] R. Khan *et al.*, "3D hierarchical heterostructured LSTN@ NiMn-layered double hydroxide as a bifunctional water splitting electrocatalyst for hydrogen production," vol. 285, p. 119174, 2021.

[170] R. Qiang *et al.*, "Electromagnetic functionalized Co/C composites by in situ pyrolysis of metal-organic frameworks (ZIF-67)," vol. 681, pp. 384-393, 2016.

[171] J. Diao *et al.*, "Interfacial engineering of W2N/WC heterostructures derived from solid-state synthesis: a highly efficient trifunctional electrocatalyst for ORR, OER, and HER," vol. 32, no. 7, p. 1905679, 2020.

[172] Z. Chen, M. Qin, P. Chen, B. Jia, Q. He, and X. J. I. J. o. H. E. Qu, "Tungsten carbide/carbon composite synthesized by combustion-carbothermal reduction method as electrocatalyst for hydrogen evolution reaction," vol. 41, no. 30, pp. 13005-13013, 2016.

[173] Y. Ling *et al.*, "Tungsten carbide hollow microspheres with robust and stable electrocatalytic activity toward hydrogen evolution reaction," vol. 4, no. 2, pp. 4185-4191, 2019.

[174] S. Lu *et al.*, "Boosting oxygen evolution through phase and electronic modulation of highly dispersed tungsten carbide with nickel doping," vol. 585, pp. 258-266, 2021.

[175] X. Ma, *Advanced Energy Efficiency Technologies for Solar Heating, Cooling and Power Generation*. Springer, 2019.

[176] J. Chen, B. Ren, H. Cui, and C. J. S. Wang, "Constructing pure phase tungsten-based bimetallic carbide nanosheet as an efficient bifunctional electrocatalyst for overall water splitting," vol. 16, no. 23, p. 1907556, 2020.

[177] J. Liang and D. W. J. A. E. M. Wang, "Design rationale and device configuration of lithium-ion capacitors," vol. 12, no. 25, p. 2200920, 2022.

[178] L. Bu *et al.*, "Supersensitive detection of chloramphenicol with an EIS method based on molecularly imprinted polypyrrole at UiO-66 and CDs modified electrode," vol. 179, p. 107459, 2022.

[179] P. Connor, J. Schuch, B. Kaiser, and W. J. Z. f. P. C. Jaegermann, "The determination of electrochemical active surface area and specific capacity revisited for the system MnOx as an oxygen evolution catalyst," vol. 234, no. 5, pp. 979-994, 2020.